

MODELLING RADIO IMAGING METHOD DATA USING ELECTRIC DIPOLES IN A  
HOMOGENOUS WHOLE SPACE

by

Tomas Naprstek

A thesis submitted in partial fulfillment  
of the requirements for the degree of  
Master of Science (MSc) in Geology

The Faculty of Graduate Studies  
Laurentian University  
Sudbury, Ontario, Canada

© Tomas Naprstek, 2014

**THESIS DEFENCE COMMITTEE/COMITÉ DE SOUTENANCE DE THÈSE**  
**Laurentian University/Université Laurentienne**  
**Faculty of Graduate Studies/Faculté des études supérieures**

Title of Thesis Titre de la thèse	MODELLING RADIO IMAGING METHOD DATA USING ELECTRIC DIPOLES IN A HOMOGENOUS WHOLE SPACE		
Name of Candidate Nom du candidat	Naprstek, Tomas		
Degree Diplôme	Master of Science		
Department/Program Département/Programme	Geology	Date of Defence Date de la soutenance	October 1, 2014

**APPROVED/APPROUVÉ**

Thesis Examiners/Examineurs de thèse:

Dr. Richard Smith  
(Supervisor/Directeur de thèse)

Mr. Alan King  
(Committee member/Membre du comité)

Mr. Damien Duff  
(Committee member/Membre du comité)

Approved for the Faculty of Graduate Studies  
Approuvé pour la Faculté des études supérieures  
Dr. David Lesbarrères  
M. David Lesbarrères  
Acting Dean, Faculty of Graduate Studies  
Doyen intérimaire, Faculté des études supérieures

Dr. Karl Butler  
(External Examiner/Examineur externe)

**ACCESSIBILITY CLAUSE AND PERMISSION TO USE**

I, **Tomas Naprstek**, hereby grant to Laurentian University and/or its agents the non-exclusive license to archive and make accessible my thesis, dissertation, or project report in whole or in part in all forms of media, now or for the duration of my copyright ownership. I retain all other ownership rights to the copyright of the thesis, dissertation or project report. I also reserve the right to use in future works (such as articles or books) all or part of this thesis, dissertation, or project report. I further agree that permission for copying of this thesis in any manner, in whole or in part, for scholarly purposes may be granted by the professor or professors who supervised my thesis work or, in their absence, by the Head of the Department in which my thesis work was done. It is understood that any copying or publication or use of this thesis or parts thereof for financial gain shall not be allowed without my written permission. It is also understood that this copy is being made available in this form by the authority of the copyright owner solely for the purpose of private study and research and may not be copied or reproduced except as permitted by the copyright laws without written authority from the copyright owner.

## **Abstract**

Information as to how the signal of the Radio Imaging Method (RIM) changes when the system parameters change or the rock properties change is not well documented. Having a better understanding of the impact of these changes would assist in the design of surveys and the interpretations of RIM data. To quantify the impacts, a modelling program was created by representing the transmitter as an electric dipole. It outputs the amplitude and phase of the electric field in a homogeneous whole space. The system parameters were varied to investigate their effects on the measured signal. It was found that increasing the conductivity or the magnetic permeability resulted in amplitude attenuation and sharper anomalies, while increasing the dielectric permittivity resulted in increased amplitude and broader anomalies. A case study was performed using data from Drury Township, near Sudbury, Ontario, Canada. The mostly homogeneous section of field data was fit with synthetic data whose conductivity values ranged in the  $10^{-3}$  S/m magnitude. A better fit was found using a conductivity of  $3 \cdot 10^{-4}$  S/m, by increasing the relative dielectric permittivity from 1 to between 18 and 20. It was concluded that the program was effective at fitting homogeneous sections of field data, and was developed into RIM forward model software for easy use.

## Keywords

Conductivity, cross borehole, geophysics, electromagnetics, electric dipole, modelling, radio imaging method, simulation, tomography

## **Acknowledgments**

I would like to thank my supervisor, Dr. Richard Smith for his support and knowledge through the research process. His guidance and assistance was invaluable. I would also like to thank my office colleagues Christoph Schaub, Omid Mahmoodi, and Yongxing Li for their general assistance and geophysics knowledge, and specifically Christoph for his proofreading skills throughout my degree. I would like to acknowledge KGHM International, Sudbury Integrated Nickel Operations A Glencore Company, Vale, Wallbridge Mining Company, the Centre for Excellence in Mining Innovation (CEMI), the Mineral Exploration Research Centre (MERC), and NSERC for support and funding. I would also like to thank Sudbury Integrated Nickel Operations for releasing the field data I used in my case study. Finally I would like to thank my good friend Benjamin Nicholls for his assistance in brainstorming several times throughout my research.

## Table of Contents

Abstract .....	iii
Acknowledgments.....	iv
Table of Contents .....	v
List of Tables .....	vi
List of Figures .....	vii
1 Introduction.....	1
2 Method .....	4
3 Analysis.....	10
3.1 Finite Dipole.....	10
3.2 Parameter Investigation.....	15
3.2.1 Electrical properties .....	15
3.2.2 Frequency variation .....	29
3.2.3 Angles.....	35
3.3 Discussion .....	37
4 Survey from Drury, Sudbury .....	38
5 Forward Modelling Program.....	54
6 Conclusions.....	56
7 References.....	60
Appendix A: Noise Level .....	63
Appendix B: Case Study Synthetic Data Cusps .....	67
Appendix C: Frequency and Dielectric Permittivity .....	69

## List of Tables

Table 1. Standard parameter values used in calculations. ....	15
Table 2. Summary of the “Rules of Thumbs” .....	28
Table 3. Summary of the "Rules of Thumbs" in terms of $\alpha$ and $\beta$ .....	29

## List of Figures

Figure 1. The basic setup of a RIM survey. The transmitter is located in one borehole, with the receiver in another borehole. The transmitter is set at a number of locations in one hole, and a series of measurements are taken with the receiver at multiple locations in another hole. The amplitude plot is built from the receiver data, and shows conductive zones/bodies where the attenuation of the signal is greater. ....	2
Figure 2: The RIM geometric configuration, listing all variables involved in the calculations. ....	5
Figure 3. The geometric variables pertaining to the transmitter reference frame $x$ and $z$ distance values. ....	7
Figure 4. Sample of the modelling code the output showing amplitude and phase of the electric field that would be measured at receiver positions ranging from 250 m above (-250 m) to 250 m below (+250 m) the transmitter depth. This is for a parallel borehole system ( $\theta_{trans} = \theta_{receive} = 0$ ), borehole separation $x = 500$ m, conductivity = $10^{-4}$ S/m. ....	10
Figure 5. Two approximations for a 10 m finite dipole. In the top panel, the finite dipole is (poorly) approximated by a single infinitesimal dipole at the center of the 10 m finite dipole. In the bottom panel, the finite dipole is approximated by five 2m dipoles distributed evenly over the 10 m length. There are three receiver positions on the right hand side. ....	11
Figure 6: A plot depicting the difference in magnitude between a transmitter calculated as a single 10 m dipole, and a transmitter calculated as ten evenly spaced 1 m dipoles. Each curve is for a different borehole separation and/or whole-space conductivity. The cusps in the dashed and dotted cases represent a switch in the sign of the magnitude difference, as the amplitudes begin as greater than the 10 m dipole case's amplitude, before falling in magnitudes to less than that of the 10 m dipole case's amplitude. ....	13

Figure 7: A convergence test for the finite dipole transmitter investigation, where the vertical boreholes are separated by 400 m, the conductivity is  $10^{-1}$  S/m and the transmitter dipole is 10 m. The component size was reduced until approximate convergence was reached. The y-axis shows the difference in amplitude between each size and the 10 m component size. It is calculated for three different points along the receiver borehole, 250 m above the transmitter, 150 m above the transmitter, and 50 m above the transmitter..... 14

Figure 8. Changes in amplitude of the electric field as a function of receiver depth for three significantly different values of distance between boreholes ( $x$  distance)..... 16

Figure 9. Changes in phase of the electric field as a function of receiver depth for three significantly different values of distance between boreholes ( $x$  distance)..... 17

Figure 10. Changes in phase of the electric field as a function of receiver depth for three slightly different values of distance between boreholes ( $x$  distance)..... 18

Figure 11. Changes in amplitude of the electric field as a function of receiver depth for three significantly different conductivity values. At  $1 \cdot 10^{-2}$  S/m, the amplitude is far below realistic detection limit. .... 19

Figure 12. Changes in phase of the electric field as a function of receiver depth for three significantly different conductivity values..... 20

Figure 13. Changes in phase of the electric field as a function of receiver depth for three slightly different conductivity values..... 21

Figure 14. Changes in amplitude of the electric field as a function of receiver depth for three significantly different dielectric permittivity values..... 22

Figure 15. Changes in phase of the electric field as a function of receiver depth for three significantly different dielectric permittivity values..... 23

Figure 16. Changes in amplitude of the electric field as a function of receiver depth for three slightly different dielectric permittivity values.....	24
Figure 17. Changes in amplitude of the electric field as a function of receiver depth for three significantly different magnetic permeability values.....	25
Figure 18. Changes in phase of the electric field as a function of receiver depth for three significantly different magnetic permeability values.....	26
Figure 19. Changes in amplitude of the electric field as a function of receiver depth for three slightly different magnetic permeability values.....	27
Figure 20: The peak amplitudes of four frequencies as a function of the distance between boreholes. This is for a parallel borehole system, with a conductivity of $10^{-4}$ S/m.....	30
Figure 21: The peak amplitudes of four frequencies as a function of the conductivity. This is for a parallel borehole system, with the distance between boreholes set to 500m. ....	31
Figure 22. The peak amplitudes of four frequencies as a function of the distance between boreholes. This is for a parallel borehole system, with a conductivity of $10^{-5}$ S/m.....	32
Figure 23. Conductivity versus $x$ distance plot, showing the frequency in each region with the greatest amplitude at that combination of values for the two parameters. A sensitivity of 25% is also added, such that any other frequency that is within 25% of the greatest amplitude will also be shown. ....	33
Figure 24. Conductivity versus $x$ distance plot, showing the frequency in each region whose amplitude exceeds its roughly estimated noise level at that combination of values for the two parameters. ....	34
Figure 25. The two angled borehole geometries used for the simulations in Figure 26.....	35

Figure 26. (top) A comparison of the amplitudes between a parallel borehole system (solid line), a system with the receiver borehole at an angle of 20 degrees (dash line), and a system with the transmitter borehole at an angle of 20 degrees (dash-dot line).....	36
Figure 27. The peak amplitude and peak position as a function of the borehole angle. The peak position is measured with respect to the position directly across from the transmitter where the zero degree peak occurs. This is for a $10^{-4}$ S/m whole space with the distance between boreholes set to 500m.....	37
Figure 28. The 625 kHz resistivity tomogram.....	40
Figure 29. The 1250 kHz resistivity tomogram.....	41
Figure 30. The 2500 kHz resistivity tomogram.....	42
Figure 31. The modelling program recreation of the geometric system in the Drury RIM data collection.....	44
Figure 32. Model and real data comparisons, with the transmitter at -275 m in borehole DR-160, frequency = 625 kHz. The model conductivity is set to $2.1 \cdot 10^{-3}$ S/m. ....	46
Figure 33. Model and real data comparisons, with the transmitter at -275 m in borehole DR-160, frequency = 1250 kHz. The model conductivity is set to $3 \cdot 10^{-3}$ S/m. ....	47
Figure 34. Model and real data comparisons, with the transmitter at -275 m in borehole DR-160, frequency = 2500 kHz. The model conductivity is set to $9 \cdot 10^{-3}$ S/m. ....	48
Figure 35. Model and real data comparisons, with the transmitter at -275 m in borehole DR-160, frequency = 625 kHz. The model conductivity is set to $3 \cdot 10^{-4}$ S/m, and the relative dielectric permittivity is set to 19.5. ....	51

Figure 36. Model and real data comparisons, with the transmitter at -275 m in borehole DR-160, frequency = 1250 kHz. The model conductivity is set to  $3 \cdot 10^{-4}$  S/m, and the relative dielectric permittivity is set to 17.3. .... 52

Figure 37. Model and real data comparisons, with the transmitter at -275 m in borehole DR-160, frequency = 2500 kHz. The model conductivity is set to  $3 \cdot 10^{-4}$  S/m, and the relative dielectric permittivity is set to 18. .... 53

Figure 38. An example of the Python GUI. .... 55

Figure 39. An example of the forward model capability of SIRIM. The black line is the synthetic data, and the red line is the imported field data. .... 56

Figure 40. Example of the comparison of the synthetic data amplitude and the field data amplitude with the transmitter at -275 m in borehole DR-160, frequency = 1250 kHz. The model conductivity is set to  $3 \cdot 10^{-4}$  S/m, and the relative dielectric permittivity is set to 17.3. The arrows show the points of comparison used. .... 64

Figure 41. Example of the noise level estimate, using the 1250 kHz data with the transmitter at -275 m in borehole DR-160. Noise here is at approximately  $10^3$  uncalibrated units. .... 65

Figure 42. The measured real and imaginary components for the synthetic data from Figure 32. .... 67

Figure 43. The measured  $z$  and  $x$  components for the synthetic data from Figure 32. .... 68

Figure 44. The peak amplitudes of four frequencies as a function of the relative dielectric permittivity. This is for a parallel borehole system, with the distance between boreholes set to 500 m, and a conductivity of  $10^{-4}$  S/m. .... 70

Figure 45. The peak amplitudes of four frequencies as a function of the relative dielectric permittivity. This is for a parallel borehole system, with the distance between boreholes set to 500 m, and a conductivity of  $10^{-5}$  S/m..... 71

Figure 46. The peak amplitudes of four frequencies as a function of the relative dielectric permittivity. This is for a parallel borehole system, with the distance between boreholes set to 500 m, and a conductivity of  $10^{-3}$  S/m..... 72

## **1 Introduction**

The radio imaging method (RIM) is a tomographic geophysical method that can be used to map electromagnetic properties in areas of interest between boreholes. Developed for the coal mining industry (Stolarczyk and Fry, 1986), RIM has since been applied with some success in several other areas, including mineral exploration and delineation (Thomson et al., 1992; Fullagar et al., 2000), and characterization of rock (Zhou and Fullagar, 2001; Korpisalo and Heikkinen, 2014). RIM is effective at locating areas of high conductivity which can be indicative of sulphide-bearing zones. The conductive medium causes the electromagnetic (EM) radiation emitted by the transmitter to attenuate, while resistive zones allow the radiation to propagate without attenuation. Zones of strong attenuation indicate an area of potential interest (Zhou et al., 1998; Stevens et al., 2000).

RIM surveys are conducted by placing a transmitter antenna down a borehole, and at a number of set locations, radio-frequency radiation is emitted (Figure 1). This is received by an antenna at multiple locations in another borehole, and the resulting signals can be used to determine features of the material between the two boreholes. In the mining industry the results can be used to focus the drilling where potential targets may be. Alternatively, if there is confidence in the RIM results, further drilling could be minimized or avoided (Mutton, 2000).

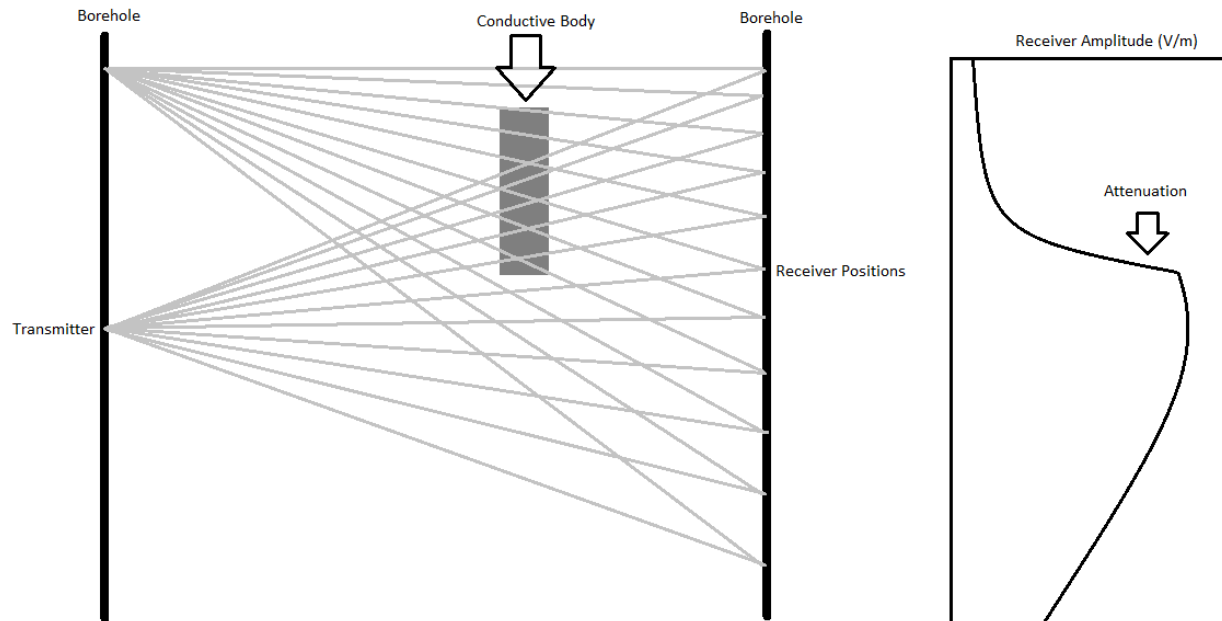


Figure 1. The basic setup of a RIM survey. The transmitter is located in one borehole, with the receiver in another borehole. The transmitter is set at a number of locations in one hole, and a series of measurements are taken with the receiver at multiple locations in another hole. The amplitude plot is built from the receiver data, and shows conductive zones/bodies where the attenuation of the signal is greater.

Much of the work that has been done on simulating and modelling RIM tends to focus on tomographic image creation (Pears and Fullagar, 1998; Karimi Sharif, 2013) and the propagation of the radiation (Johnson, 1997; Jang et al., 2006). The tomographic processing efforts are typically in raypath inversion, where the subsurface is divided into small “blocks”, each with their own attenuation/conductivity value. The radiation propagation work is generally focused on creating finite difference time domain (FDTD) simulations to understand how the radiation will be affected by inhomogeneity, antennae spacing, water-filled boreholes, and other factors that can affect the transmission of radio-frequency radiation. How the radiation is reflected, absorbed,

and re-emitted is important to understand in RIM and assists in interpretation of RIM data. However, there is less research in radiation propagation done in the context of the received signal, and the effects of the physical and geometric parameters of the system that affect RIM.

As such, this research was carried out with the goal of better understanding the electric field that would be measured at the receivers, based on the parameters of the whole-space model and the system geometry.

The representation of the transmitter as a single infinitesimal dipole is an assumption used (Holliger et al., 2001) in much of RIM research. The validity of this approximation was investigated by constructing a larger dipole of multiple infinitesimal dipoles.

The borehole separation, conductivity, dielectric permittivity, magnetic susceptibility, frequency of the transmitter, and angles of the boreholes were all parameters which were analyzed to understand their effects on the amplitude and phase. Understanding how the signal changes when a single one of these system parameters is varied will allow an understanding of how each of the parameters can affect data. Furthermore, the complex interaction of how each parameter may accentuate or reduce the effect of another parameter was investigated.

This knowledge will allow more confidence in results, as well as assist in interpretations of an area that is being surveyed by RIM. Additionally, this research has led to the creation of basic forward model software specifically for RIM survey data.

## 2 Method

To investigate the signal of RIM data, a whole-space modelling program was created in Matlab<sup>®</sup> using the formulation of Ward and Hohmann (1987). The program simulates the transmitter as an electric dipole in a homogeneous whole space, and calculates the resulting electric field that would be measured in a receiver borehole, as a function of the parameters of the whole space and the system geometry (Figure 2). By varying parameters of the model, it is possible to gain an understanding of how the signal changes, which can ultimately assist in creating more accurate inversions and interpretations.

The mathematical formula describing the electric field  $\mathbf{E}$  of a  $z$ -directed electric dipole associated with this model is Equation 1 (adapted from Ward and Hohmann, 1987, p.173, and additional description from Zhou and Fullagar, 2001):

$$\mathbf{E} = \frac{I ds}{4\pi\sigma r^3} e^{-ikr} \left[ \left( \frac{z^2}{r^2} \mathbf{u}_z + \frac{zy}{r^2} \mathbf{u}_y + \frac{zx}{r^2} \mathbf{u}_x \right) (-k^2 r^2 + 3ikr + 3) + (k^2 r^2 - ikr - 1) \mathbf{u}_z \right], \quad (1)$$

where:

$$r = \sqrt{x^2 + y^2 + z^2}, \quad (2)$$

$$k = \alpha - i\beta, \text{ is the complex wavenumber,} \quad (3)$$

$$\alpha = \omega \left\{ \frac{\mu\epsilon}{2} \left[ \left( 1 + \frac{\sigma^2}{\epsilon^2 \omega^2} \right)^{1/2} + 1 \right] \right\}^{1/2}, \text{ is the wavenumber/phase coefficient} \quad (4)$$

and

$$\beta = \omega \left\{ \frac{\mu\epsilon}{2} \left[ \left( 1 + \frac{\sigma^2}{\epsilon^2 \omega^2} \right)^{1/2} - 1 \right] \right\}^{1/2}, \text{ is the attenuation rate/absorption coefficient} \quad (5)$$

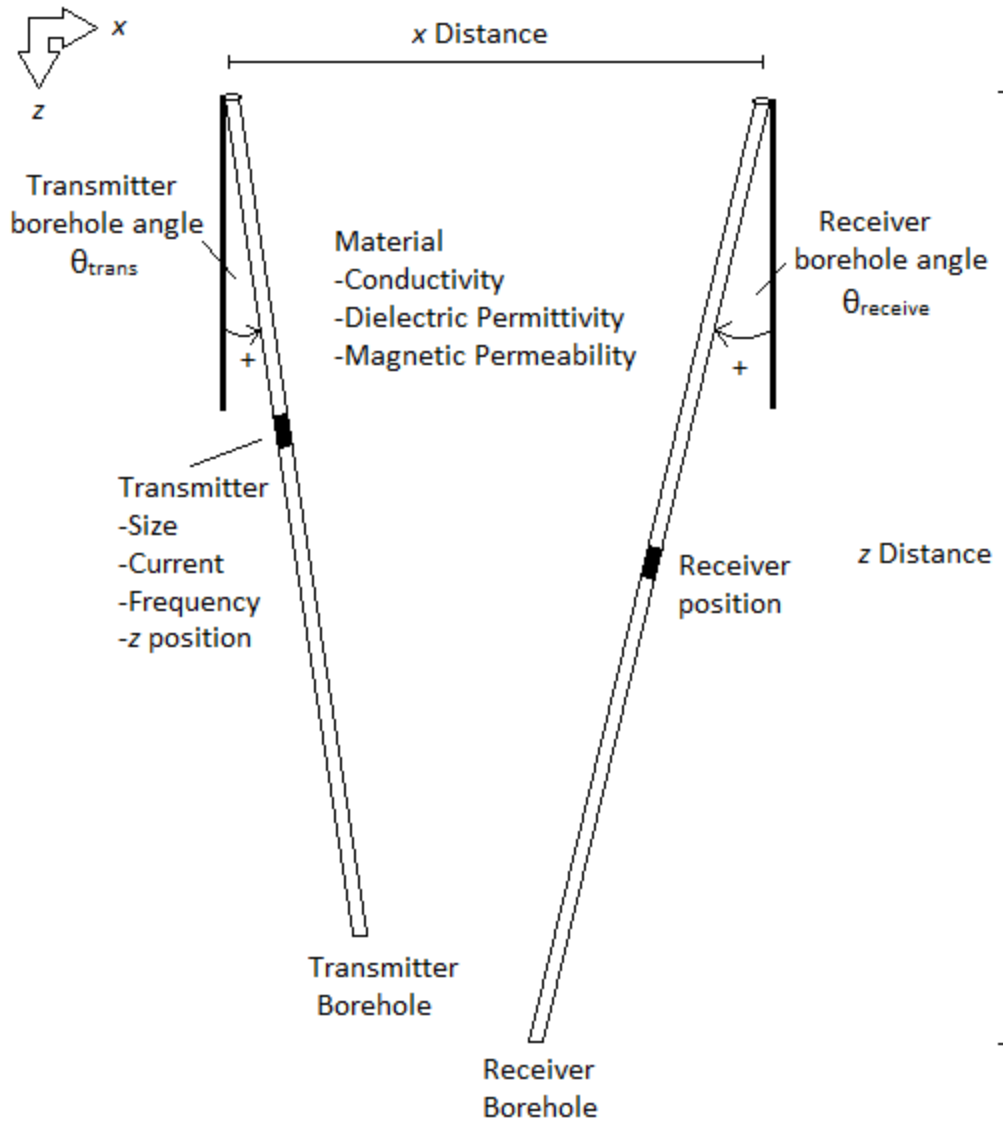


Figure 2: The RIM geometric configuration, listing all variables involved in the calculations.

$I$  is the current (A),  $ds$  is the size of the transmitter (m),  $\sigma$  is the conductivity (S/m),  $\omega$  is the angular frequency (radians/s) dependent on the transmitter frequency (Hz),  $\epsilon$  is the dielectric permittivity (F/m),  $\mu$  is the magnetic permeability (H/m), and  $u_i$  is the unit vector in the  $i^{\text{th}}$  direction.

This equation was adapted from the  $x$ -directed dipole given by Ward and Hohmann by switching variables and ensuring a right-hand-coordinate system. In cases when the borehole containing the receiver is not vertical, the  $z$  axis of the electric field is rotated to lie along the axis of the borehole. For the purposes of this modelling program, the boreholes are always in the same  $y$  plane, and therefore there is no  $y$  distance. Though  $\alpha$  and  $\beta$  can generally be simplified (Fullagar et al., 2000), no approximations were made in this analysis. Also note that the wavelength in the medium can be calculated from  $\alpha$ :

$$\lambda = \frac{2\pi}{\alpha}. \quad (6)$$

The whole-space modelling software was designed to calculate the real and imaginary parts of the  $z$  and  $x$  components of the electric field every 1 m down the receiver borehole, resulting in four values for every position, which are eventually converted to the measured amplitude and phase. Two reference frames are required for these calculations: the absolute reference frame and the transmitter reference frame. If the transmitter borehole is on an angle, then the electromagnetic field being generated is on an angle as well, and must be taken into account (Figure 3).

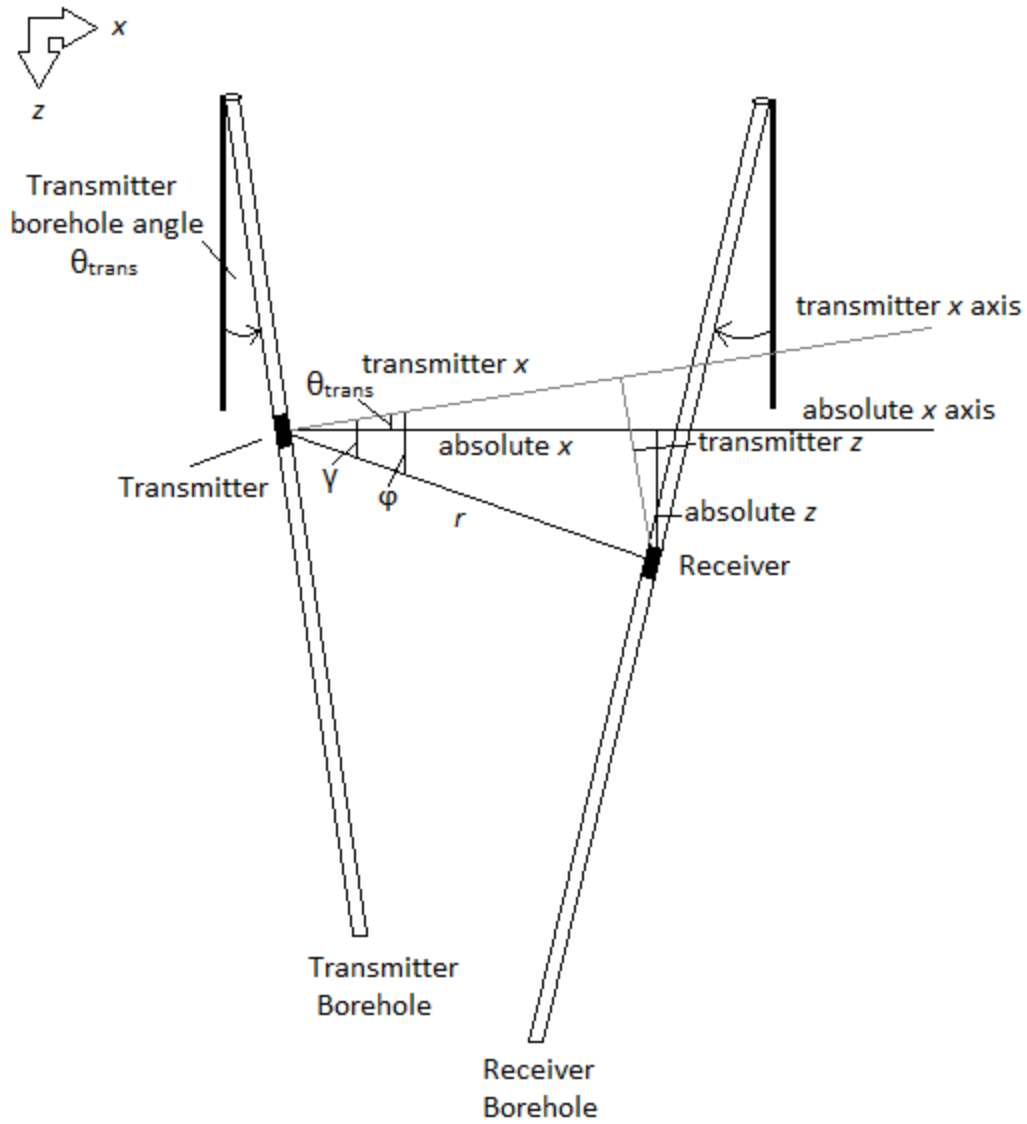


Figure 3. The geometric variables pertaining to the transmitter reference frame  $x$  and  $z$  distance values.

To do this, first the  $x$  and  $z$  distances between the transmitter and the receiver are calculated in the absolute reference frame based on the angles and distances given by the user. The  $x$  distance is calculated as follows:

$$x_{absolute\ distance} = x_{top} - ((z_{current}) \tan \theta_{receive}) - ((z_{source}) \tan \theta_{trans}), \quad (7)$$

$x_{top}$  is the  $x$  distance between boreholes at the top of the model,  $z_{current}$  is the current receiver  $z$  position being calculated,  $z_{source}$  is the  $z$  position of the transmitter vertically,  $\theta_{trans}$  is the angle of the transmitter borehole with respect to the vertical, and  $\theta_{receive}$  is the angle of the receiver borehole with respect to the vertical. For both angles, a positive angle specifies the borehole being rotated towards the center of the system (bottom of the hole rotated in), while a negative angle specifies the borehole being rotated away from the center of the system (rotated out). In other words, for the right borehole, a positive angle is a clockwise rotation and for the left it is counter-clockwise. The transmitter is always assumed to be on the left side.

The depth of the receiver is measured relative to the position of the transmitter, with negative depths referring to depths above the transmitter, in the ground reference system:

$$z_{absolute\ distance} = z_{current} - z_{source}, \quad (8)$$

Using the  $x$  and  $z$  distances, the angle  $\gamma$  between the direct path from transmitter to receiver (referred to as  $r$ ) and the absolute  $x$  axis is given by:

$$\gamma = \tan^{-1} \left( \frac{z_{absolute\ distance}}{x_{absolute\ distance}} \right), \quad (9)$$

and, the angle between  $r$  and the  $x$  axis in the transmitter reference frame is given by:

$$\phi = \gamma + \theta_{trans}. \quad (10)$$

Having defined  $\phi$ , the transmitter reference frame  $x$  and  $z$  values are simply:

$$x_{trans\ distance} = r \cos \phi, \quad (11)$$

$$z_{trans\ distance} = r \sin \phi, \quad (12)$$

The component of the electric field that would be measured by a sensor oriented along the receiver borehole is then calculated, based on the angles of the boreholes in degrees:

$$E_{current} = (\cos(\theta_{trans} + \theta_{receive}))E_{current,z} + (\cos(90^\circ - \theta_{trans} + \theta_{receive}))E_{current,x}, \quad (13)$$

This is done for both real and imaginary components, and finally the total amplitude and phase angle are calculated and plotted (Figure 4).

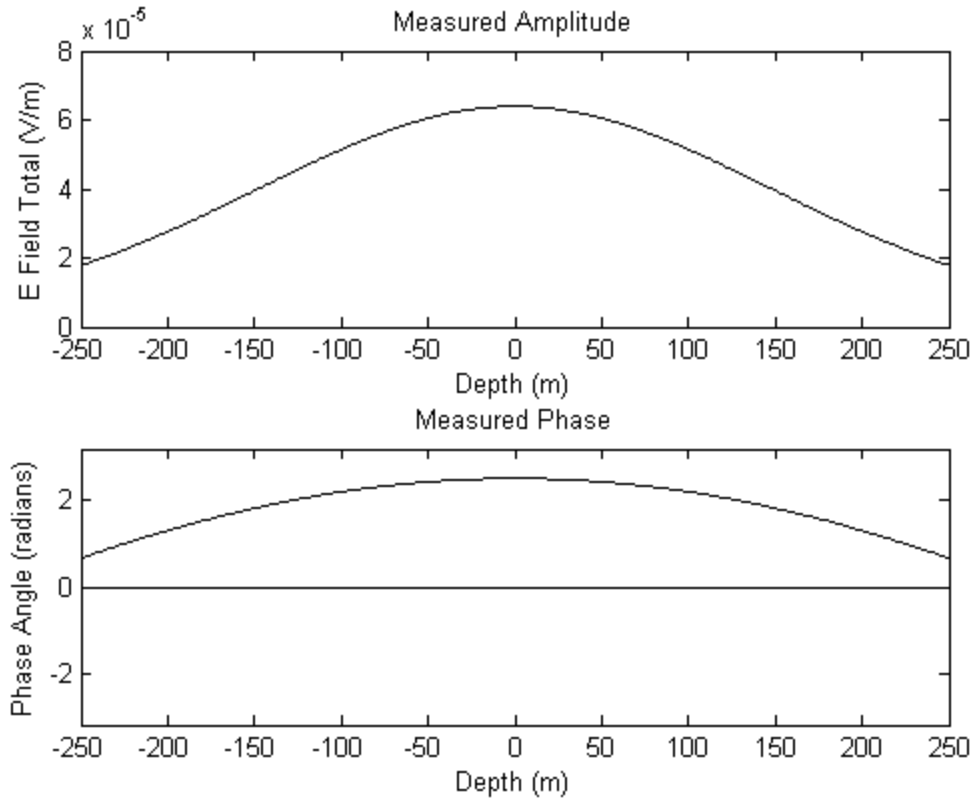


Figure 4. Sample of the modelling code the output showing amplitude and phase of the electric field that would be measured at receiver positions ranging from 250 m above (-250 m) to 250 m below (+250 m) the transmitter depth. This is for a parallel borehole system ( $\theta_{trans} = \theta_{receive} = 0$ ), borehole separation  $x = 500$  m, conductivity =  $10^{-4}$  S/m.

### 3 Analysis

#### 3.1 Finite Dipole

The transmitter is commonly assumed to be an infinitesimal dipole (Holliger et al., 2001) located at the center of the transmitter position with effective length  $ds$  (Ward and Hohmann, 1987, p.173). This is due to the relatively large distance involved in RIM surveys (usually several

hundred metres), compared to the size of the transmitter dipole (generally a few tens of metres). To test the validity of this assumption, the transmitter was given a simplified finite size by placing equal sized dipoles at points evenly distributed around the center of the finite transmitter position. This allowed a simple approximation of the geometric factors that could affect the signal, as the EM radiation would no longer be emitted from a single point, but instead several spread over a small distance (Figure 5).

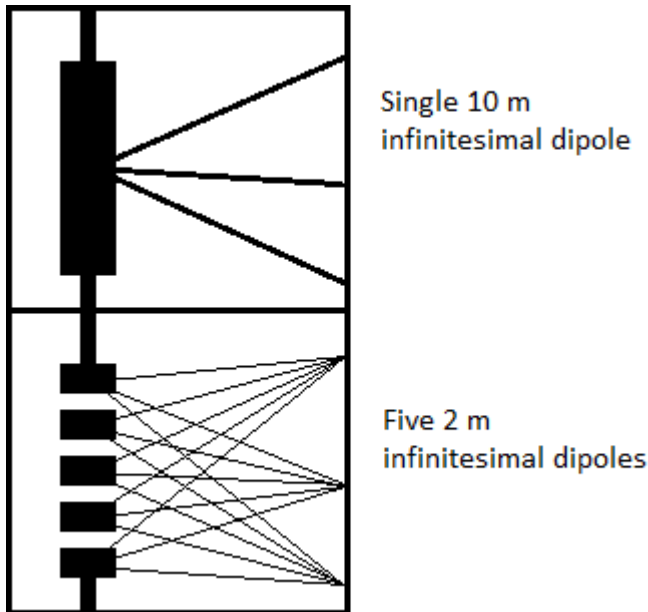


Figure 5. Two approximations for a 10 m finite dipole. In the top panel, the finite dipole is approximated by a single infinitesimal dipole at the center of the 10 m finite dipole. In the bottom panel, the finite dipole is approximated by five 2m dipoles distributed evenly over the 10 m length. There are three receiver positions on the right hand side.

The amplitudes of one infinitesimal dipole with  $ds = 10$  m used as the simplest approximation for a 10 m long transmitter, were compared with the combined amplitudes from ten dipoles with  $ds = 1$  m spread over a 10 m length for the case of two boreholes 400 m apart in a relatively resistive whole space of conductivity set to  $10^{-4}$  S/m. It was found that the amplitudes varied by a

very small factor, less than 1%. However, if the conductivity is raised to 0.1 S/m, the difference rises to as much as 20%. If the distance between boreholes is reduced to 200 m, the difference rises further, up to 50%. However, these increased differences only occurred at amplitudes that would likely be below noise levels in field data, due to the high conductivity. Figure 6 shows the errors as a function of the depth in the receiver hole.

This model of a whole space at high conductivity is unlikely to occur in a mineral exploration survey in Canada. However it can be postulated that if a large conductive body is present, it is possible that the results of an inversion may be inaccurate if a single infinitesimal dipole is assumed for the transmitter. This error may be accentuated if the borehole separation is small.

A convergence test (Figure 7) was conducted for the 0.1 S/m case to understand how the error varied as the number of dipoles used to represent the transmitter changed. The results are the difference between the amplitudes from the conventional approximation (the single dipole) case, and the smaller (and more numerous) dipoles case. The number of dipoles increases and the corresponding size of the component dipole decreases towards the left. The amplitude difference was calculated at three receiver locations to represent the complexity of the curve in Figure 6.

Splitting the transmitter into two infinitesimal dipoles, each half the size of the transmitter (5 m in this case), gives a result close to convergence, even in a very conductive environment. Further reductions to five dipoles (2 m) or 10 dipoles (1 m) do not yield a significant improvement. As such, it can be concluded that if a survey is completed in a very conductive environment, or there is a large conductive zone between closely spaced boreholes, then the transmitter should be approximated by at least two dipoles, as the lateral offset of these two dipoles can account for the geometry of a finite-sized dipole. In almost all cases however, it is unlikely that even this approximation will be necessary as in most situations any error will be insignificant.

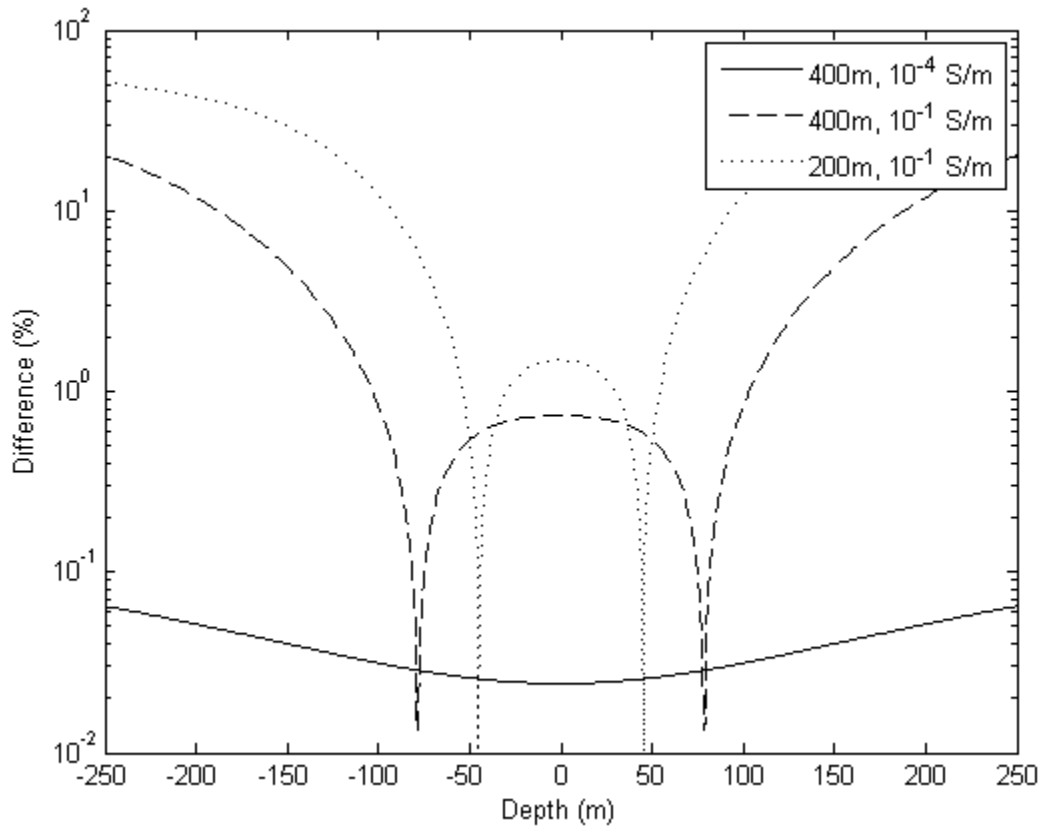


Figure 6: A plot depicting the difference in magnitude between a transmitter calculated as a single 10 m dipole, and a transmitter calculated as ten evenly spaced 1 m dipoles. Each curve is for a different borehole separation and/or whole-space conductivity. The cusps in the dashed and dotted cases represent a switch in the sign of the magnitude difference, as the amplitudes begin as greater than the 10 m dipole case's amplitude, before falling in magnitudes to less than that of the 10 m dipole case's amplitude.

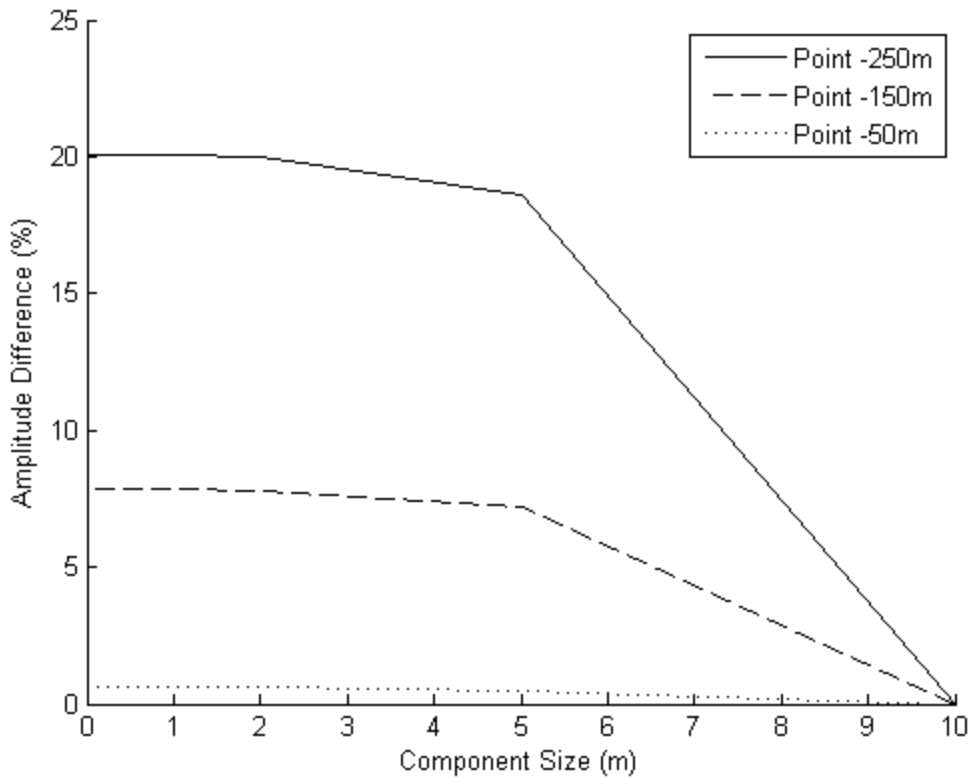


Figure 7: A convergence test for the finite dipole transmitter investigation, where the vertical boreholes are separated by 400 m, the conductivity is  $10^{-1}$  S/m and the transmitter dipole is 10 m. The component size was reduced until approximate convergence was reached. The y-axis shows the difference in amplitude between each size and the 10 m component size. It is calculated for three different points along the receiver borehole, 250 m above the transmitter, 150 m above the transmitter, and 50 m above the transmitter.

## 3.2 Parameter Investigation

### 3.2.1 Electrical properties

Another goal of this research was to investigate how the signal changes given a change in one of the variables of the system. Understanding how each parameter affects the data will assist in field data interpretation. There are many situations that can be simulated with the whole-space modelling program, and as such, the effect of a changing parameter can be documented in a controlled manner. The following plots (Figures 8 - 19) show the effect of changing a parameter on the amplitude and phase. Each parameter is varied over a large range of values, followed by a smaller range, such that the effect of the parameter on the phase can be seen at both a large and small scale.

The standard values for the parameters used in the simulation are listed in Table 1.

Table 1. Standard parameter values used in calculations.

Variable	Value
$x$ distance between holes	500 m
$z$ position of transmitter	250 m
Transmitter Size	10 m
Transmitter Component Size	1 m
Frequency	1250 kHz
Transmitter Current	10 amps
Transmitter Borehole Angle	0 degrees
Receiver Borehole Angle	0 degrees
Conductivity	$10^{-4}$ S/m
Relative Dielectric Permittivity	1
Relative Magnetic Permeability	1

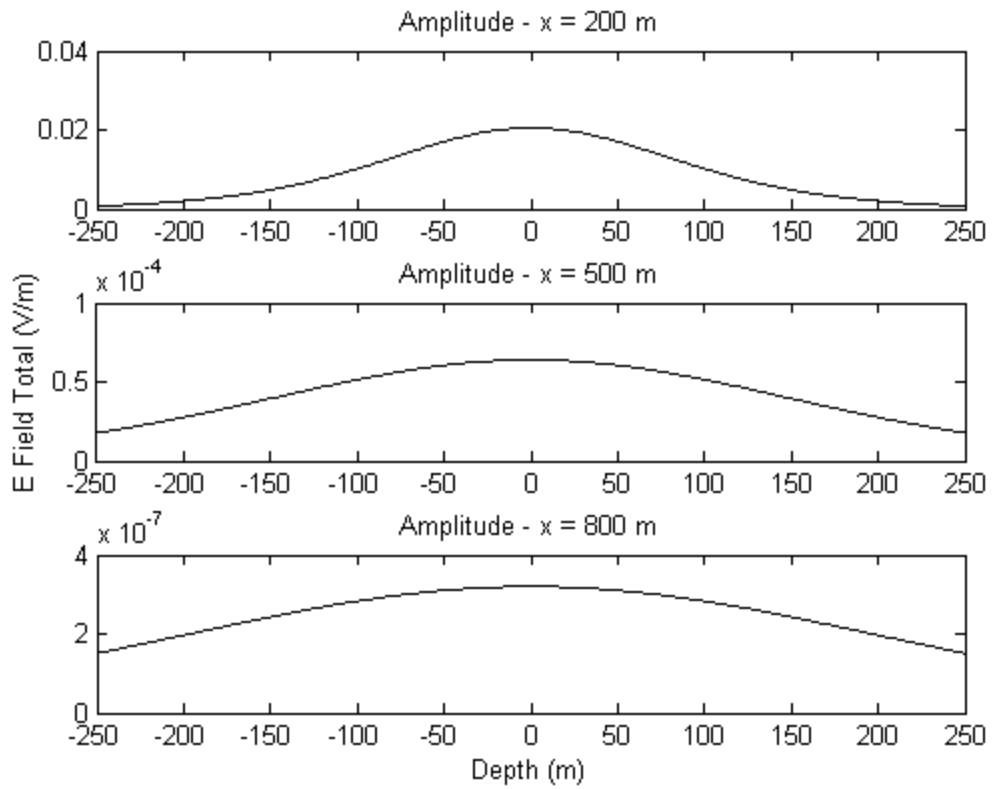


Figure 8. Changes in amplitude of the electric field as a function of receiver depth for three significantly different values of distance between boreholes ( $x$  distance).

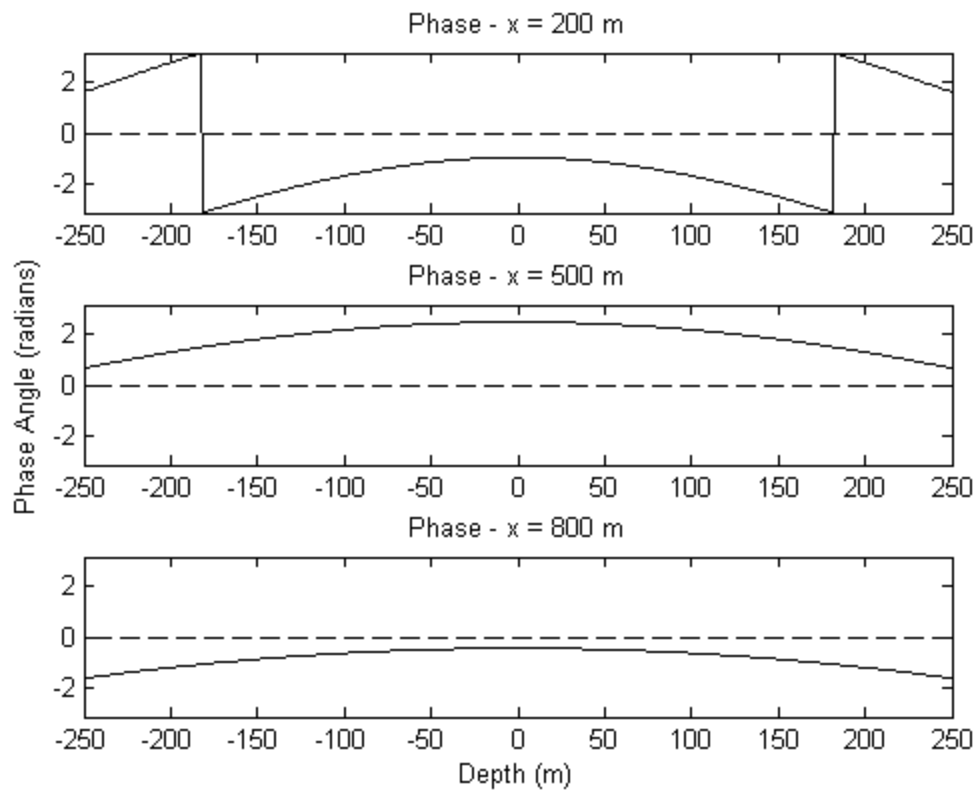


Figure 9. Changes in phase of the electric field as a function of receiver depth for three significantly different values of distance between boreholes ( $x$  distance).

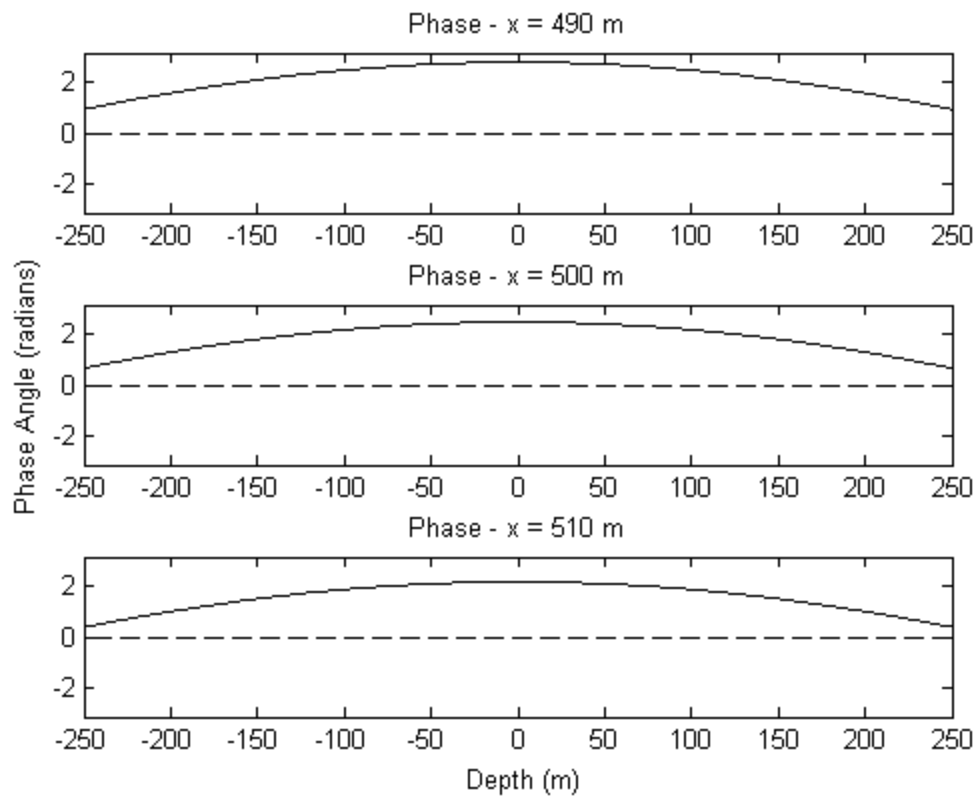


Figure 10. Changes in phase of the electric field as a function of receiver depth for three slightly different values of distance between boreholes ( $x$  distance).

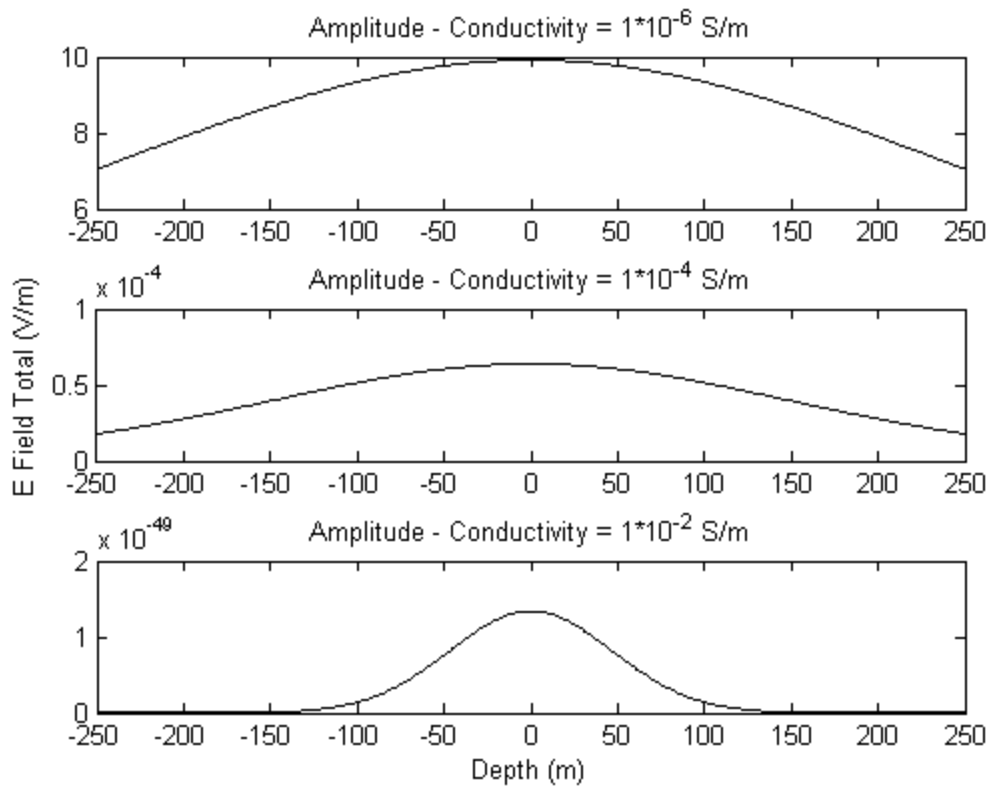


Figure 11. Changes in amplitude of the electric field as a function of receiver depth for three significantly different conductivity values. At  $1 \cdot 10^{-2}$  S/m, the amplitude is far below realistic detection limit.

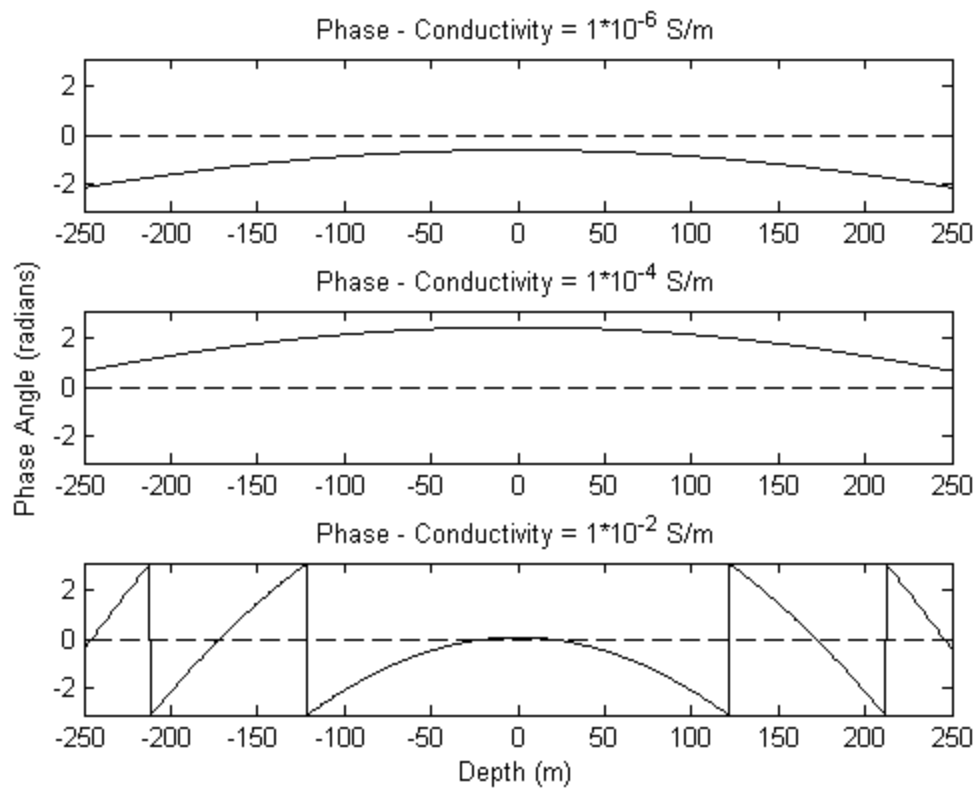


Figure 12. Changes in phase of the electric field as a function of receiver depth for three significantly different conductivity values

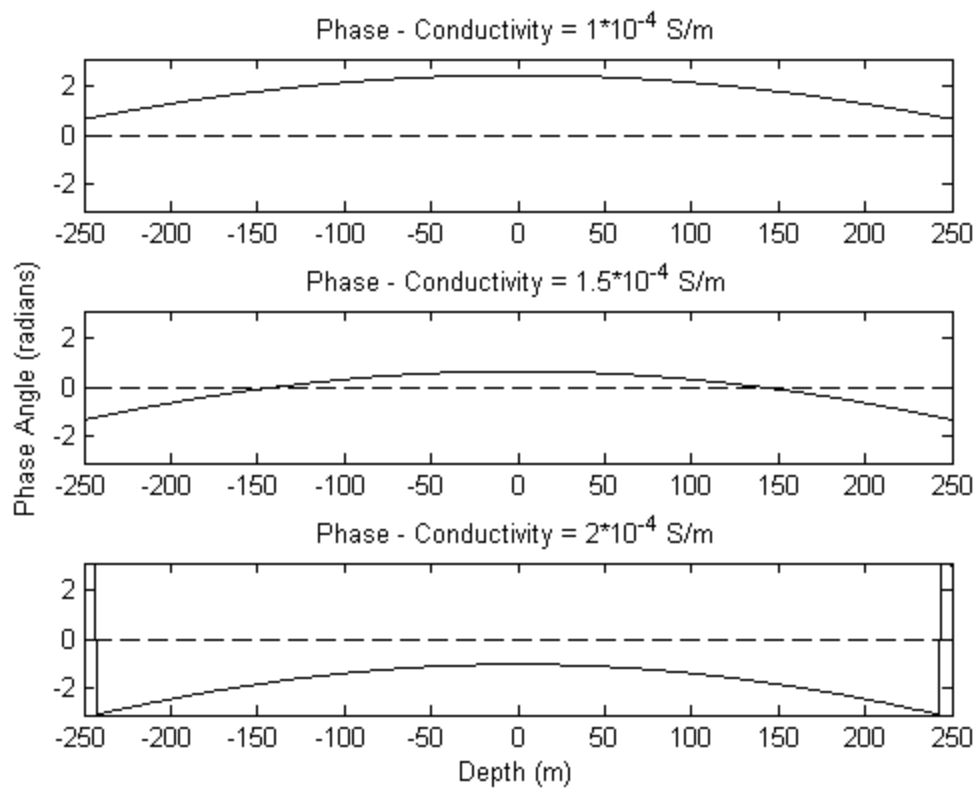


Figure 13. Changes in phase of the electric field as a function of receiver depth for three slightly different conductivity values

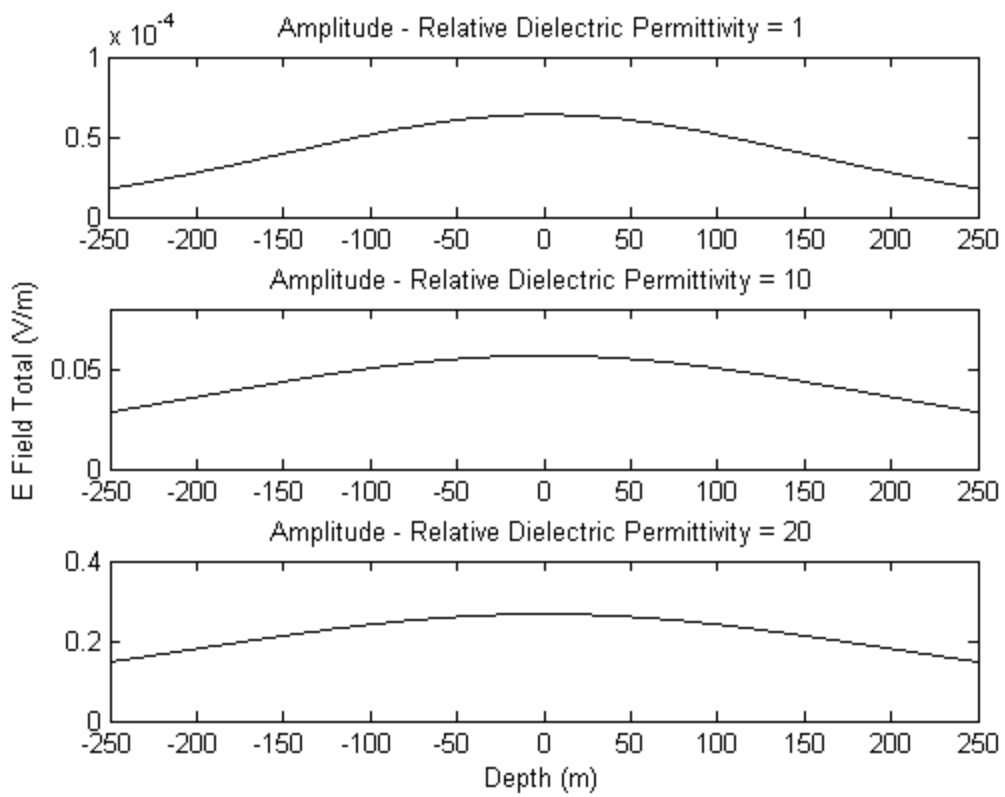


Figure 14. Changes in amplitude of the electric field as a function of receiver depth for three significantly different dielectric permittivity values.

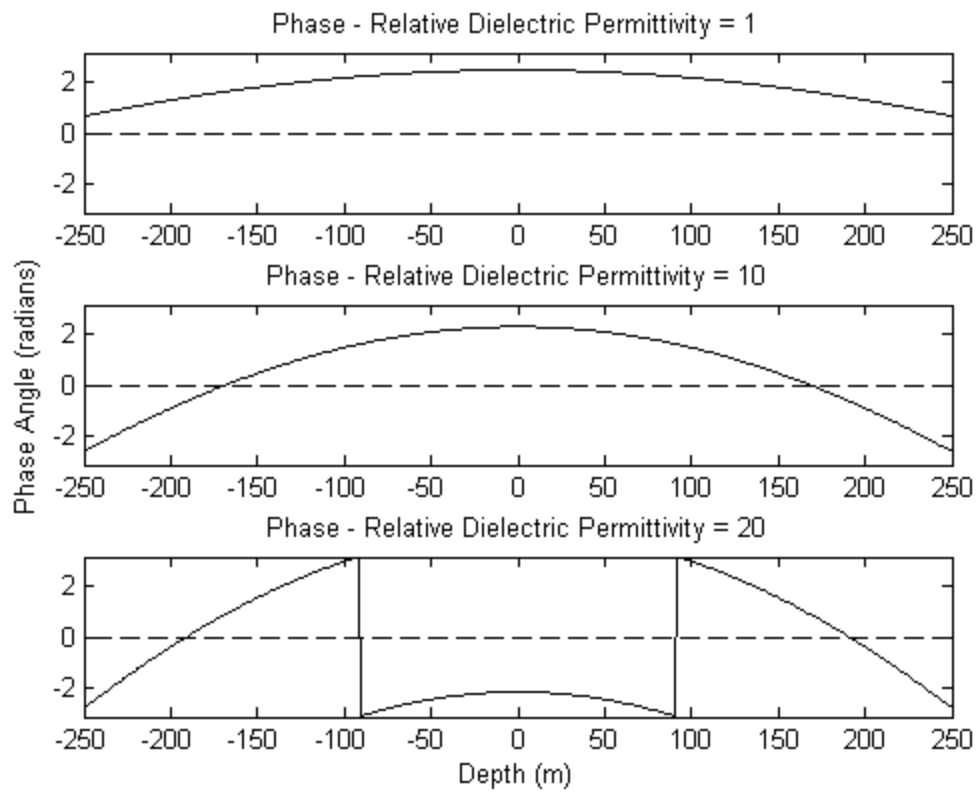


Figure 15. Changes in phase of the electric field as a function of receiver depth for three significantly different dielectric permittivity values.

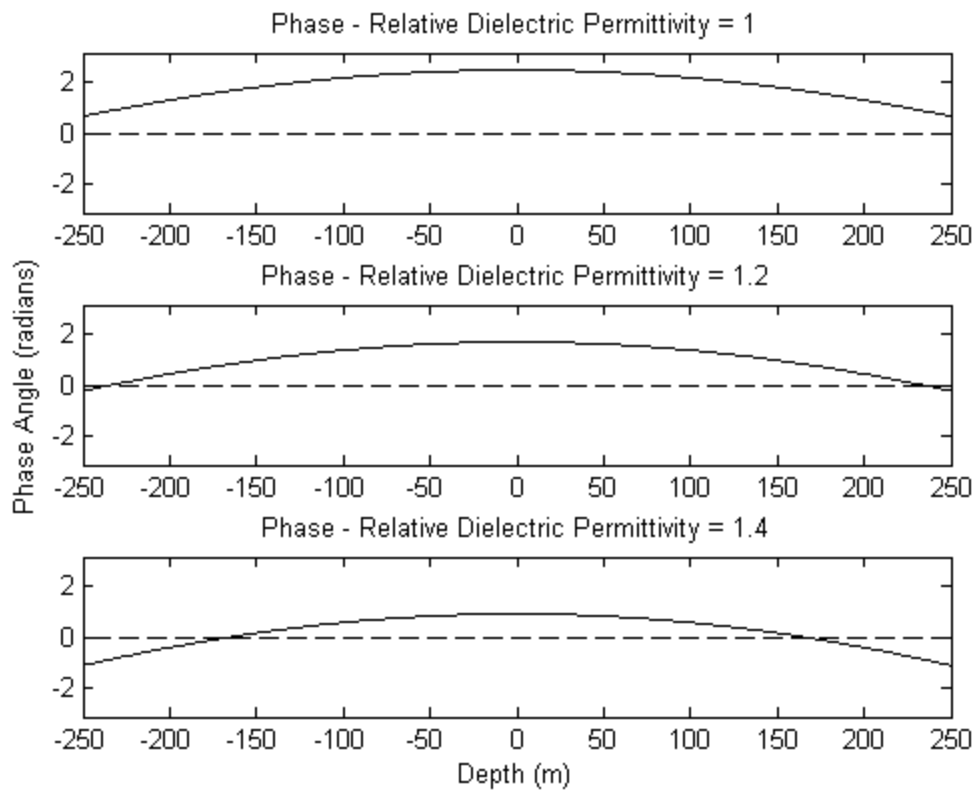


Figure 16. Changes in amplitude of the electric field as a function of receiver depth for three slightly different dielectric permittivity values.

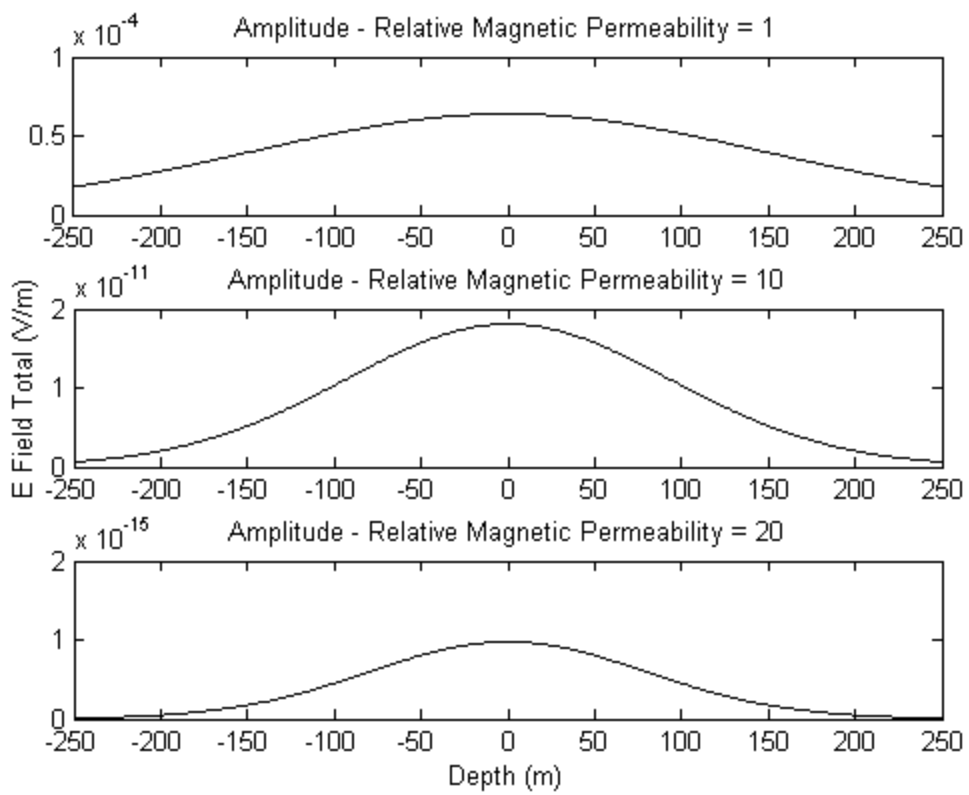


Figure 17. Changes in amplitude of the electric field as a function of receiver depth for three significantly different magnetic permeability values.

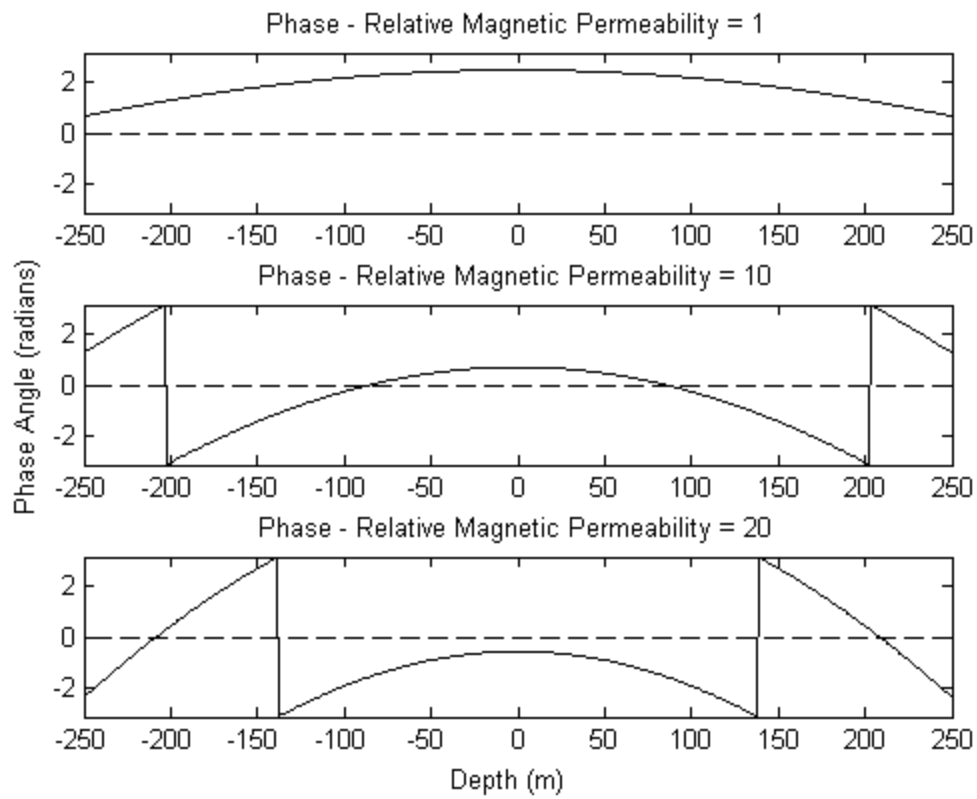


Figure 18. Changes in phase of the electric field as a function of receiver depth for three significantly different magnetic permeability values.

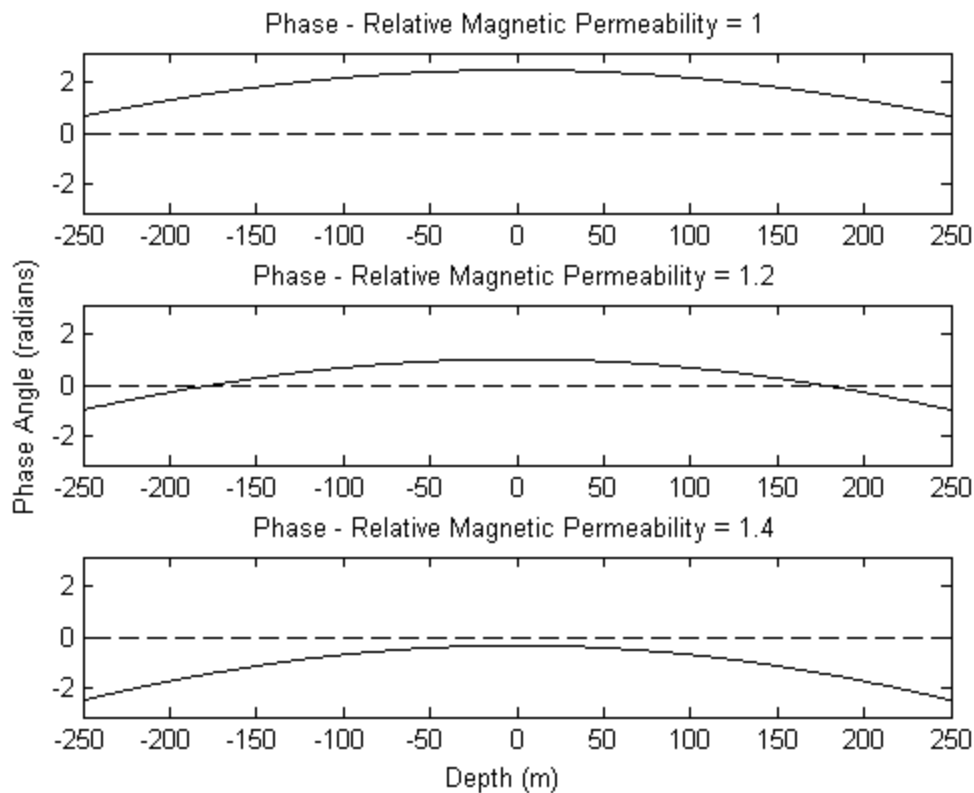


Figure 19. Changes in amplitude of the electric field as a function of receiver depth for three slightly different magnetic permeability values.

From these above plots, several patterns can be observed in the way the amplitude and phase values change when varying a single parameter. The following “rules of thumb” are concluded:

- Increasing the **borehole separation  $x$**  causes a **broadening** of the **amplitude** peak, and **decreases** the overall magnitude of amplitude (Figure 8)
- Increasing the **borehole separation  $x$**  causes a **broadening** of the **phase** peak (Figure 9), and **shifts phase negatively** (Figure 10)
- Increasing **conductivity** causes a **sharpening** of the **amplitude** peak, and **decreases** the overall magnitude of amplitude (Figure 11)

- Increasing **conductivity** causes a **sharpening** of the **phase** peak (Figure 12), and **shifts phase negatively** (Figure 13)
- Increasing the **dielectric permittivity** causes a small **broadening** of the shape of the **amplitude** peak, and **increases** the overall magnitude of the amplitude (Figure 14)
- Increasing **dielectric permittivity** causes a **sharpening** of the **phase** peak (Figure 15), and **shifts phase negatively** (Figure 16)
- Increasing **magnetic permeability** causes a **sharpening** of the **amplitude** peak, and **decreases** the overall magnitude of amplitude (Figure 17)
- Increasing **magnetic permeability** causes a **sharpening** of the **phase** peak (Figure 18), and **shifts phase negatively** (Figure 19)

These rules are summarized in Table 2 below.

Table 2. Summary of the “Rules of Thumbs”.

<b>Increasing Variable</b>	<b>Amplitude Peak</b>	<b>Amplitude Value</b>	<b>Phase Peak</b>	<b>Phase Value</b>
<b><math>x</math> distance</b>	Broadens	Decreases	Broadens	Decreases
<b>Conductivity</b>	Sharpens	Decreases	Sharpens	Decreases
<b>Dielectric Permittivity</b>	Broadens	Increases	Sharpens	Decreases
<b>Magnetic Permeability</b>	Sharpens	Decreases	Sharpens	Decreases

Another method of interpretation is to observe the change in  $\alpha$  and  $\beta$  (Table 3). Following equation (6), it can therefore be stated that increasing any of the medium’s parameters will cause a decrease in the wavelength of the EM radiation and an increase (decrease in the case of dielectric permittivity) of the attenuation.

Table 3. Summary of the "Rules of Thumbs" in terms of  $\alpha$  and  $\beta$ .

<b>Increasing Variable</b>	<b><math>\alpha</math> (Phase Coefficient)</b>	<b><math>\beta</math> (Absorption Coefficient)</b>
<b><math>x</math> distance</b>	No change	No change
<b>Conductivity</b>	Increases	Increases
<b>Dielectric Permittivity</b>	Increases	Decreases
<b>Magnetic Permeability</b>	Increases	Increases

There is some possibility of ambiguity in interpretation as similar behaviours could be ascribed to increases in conductivity or magnetic permeability. However, due to the stronger variation of the signal with changing conductivity, as well as the fact that conductivity varies over a larger range, it can be assumed that the standard conclusion of a change in RIM response being ascribed to a change in conductivity is valid in most situations. This is a possible area of further investigation.

These patterns can assist in interpretation of real data, as they can give basic explanations as to why a trend occurs in a dataset. However the degree to which these trends occur is generally dependent on the other parameters, as well as the geometry. For instance, increasing dielectric permittivity when the conductivity is low causes a much greater change in the phase as compared to when the conductivity is high. As such, these rules of thumb will generally hold true, however checking a specific situation with the modelling program will ensure a more full understanding of how the data may change. The methodology described in this thesis allows modelling of specific situations.

### **3.2.2 Frequency variation**

Different frequencies will result in different signals, and modelling can be used to determine the frequency that may be more appropriate in certain situations.

The amplitudes of four commonly used RIM frequencies were plotted against distance (Figure 20) and conductivity (Figure 21). From these plots it was found that at smaller distances and in more resistive material, 2500 kHz results in the highest amplitude, while at larger distances and more conductive systems, 312.5 kHz results in much greater amplitude than any other frequency. At large distances, 312.5 kHz has amplitude that is up to two orders of magnitude greater than the other frequencies. At no point do either of the middle two frequencies have an amplitude that is greater, as the maximum amplitude “jumps” from 2500 kHz directly to 312.5 kHz.

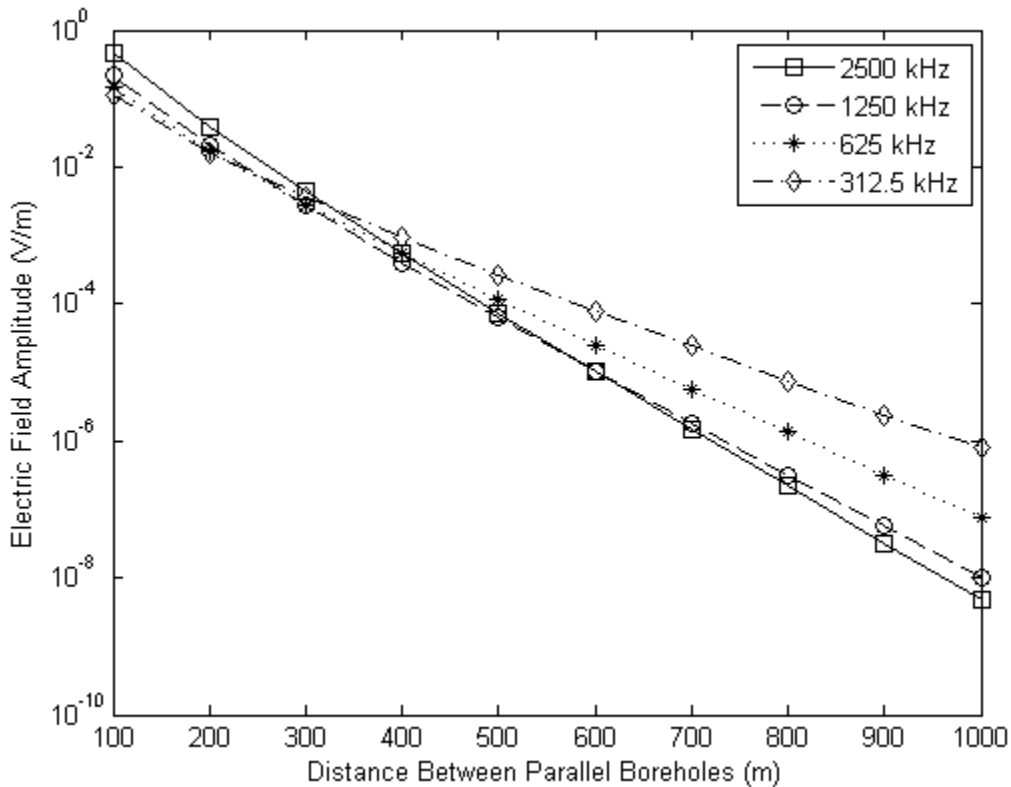


Figure 20: The peak amplitudes of four frequencies as a function of the distance between boreholes. This is for a parallel borehole system, with a conductivity of  $10^{-4}$  S/m.

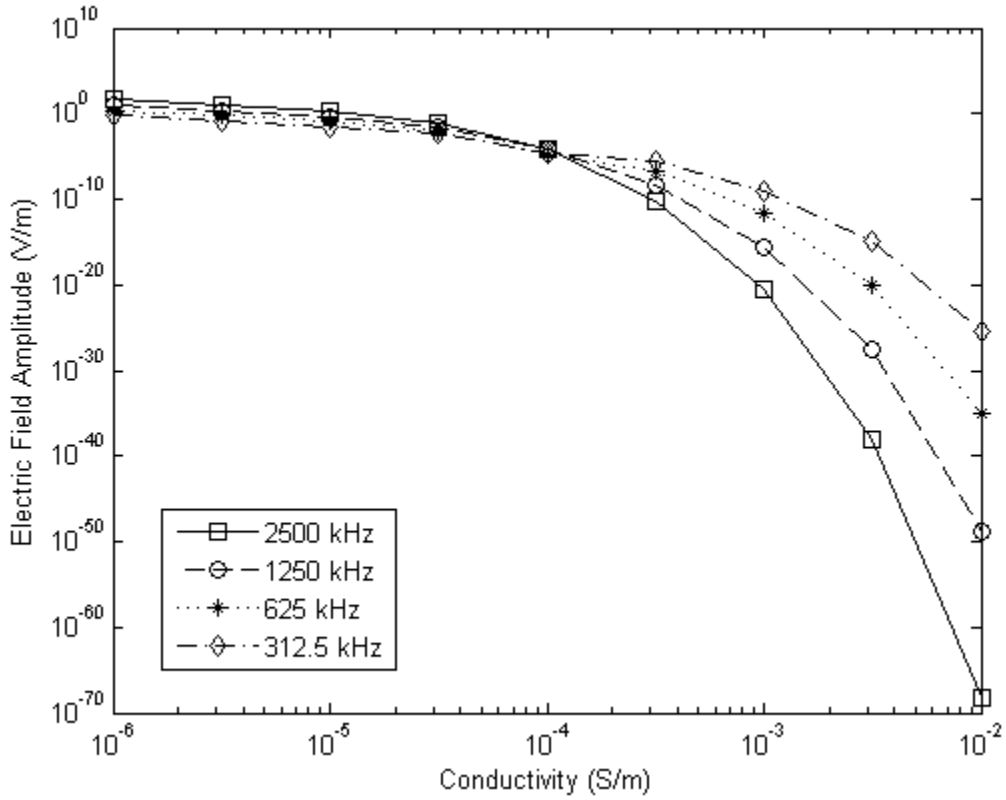


Figure 21: The peak amplitudes of four frequencies as a function of the conductivity. This is for a parallel borehole system, with the distance between boreholes set to 500m.

From the above two plots, it can be seen that at a conductivity of  $10^{-5}$  S/m, it can be expected that at all, or most distances, 2500 kHz should result in the largest amplitude. Inputting these parameters into the modelling program and plotting, it can be seen that this is true (Figure 22).

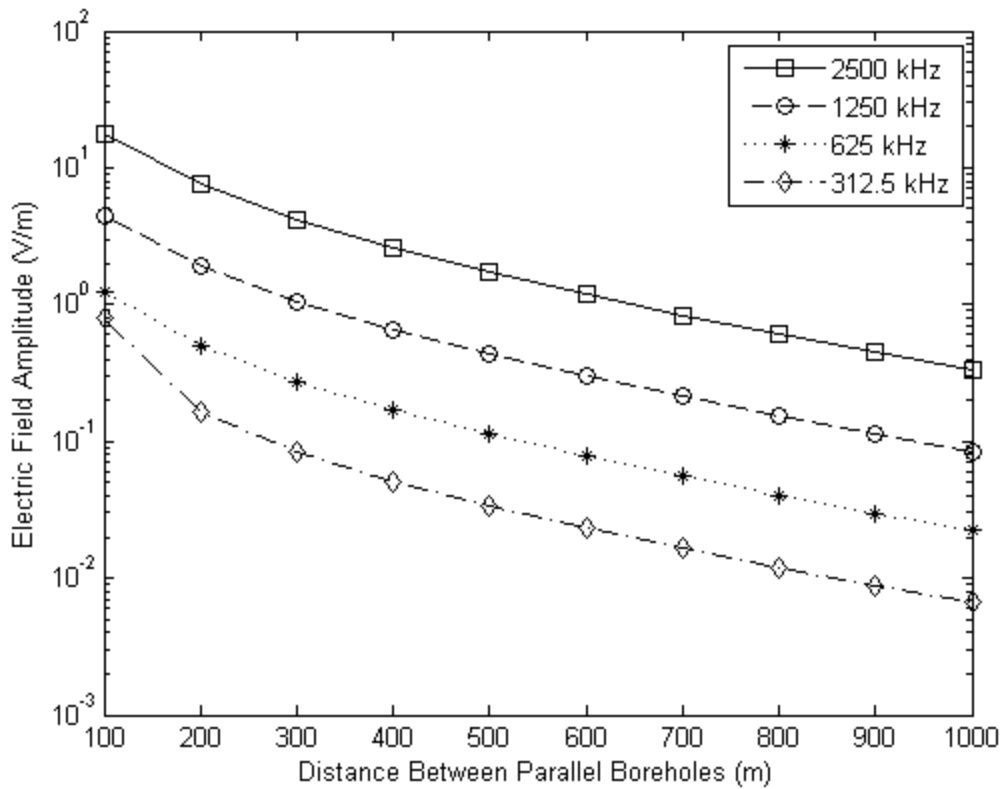


Figure 22. The peak amplitudes of four frequencies as a function of the distance between boreholes. This is for a parallel borehole system, with a conductivity of  $10^{-5}$  S/m.

To summarize these results, we plot the frequency whose amplitude is greatest, as well as any other frequency whose amplitude is similar in value on a plot for different conductivities and borehole offsets. In Figure 23, the similarity threshold is set to 0.25, such that the frequency with the maximum amplitude is shown, as well as any frequency whose amplitude is greater than or equal to 25% less than the greatest amplitude.

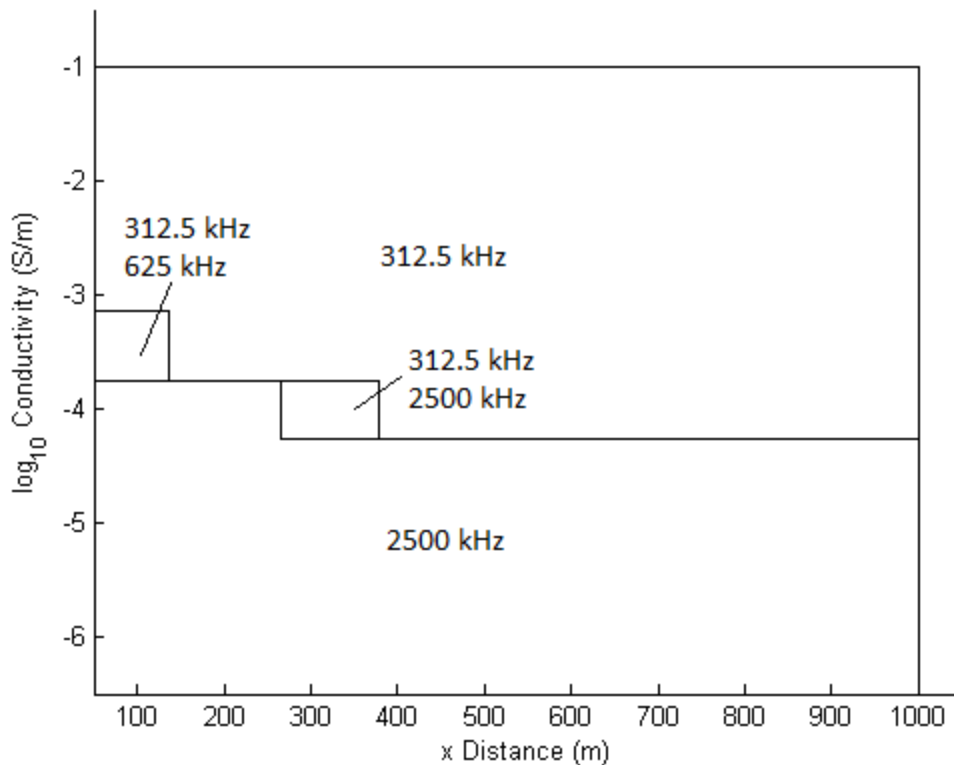


Figure 23. Conductivity versus  $x$  distance plot, showing the frequency in each region with the greatest amplitude at that combination of values for the two parameters. A sensitivity of 25% is also added, such that any other frequency that is within 25% of the greatest amplitude will also be shown.

However the above plots do not take into consideration what amplitude is realistically measurable, and what amplitudes would be above the noise level. To get a rough approximation as to what an expected noise level may be, noise values from the case study in Section 4 were estimated. For the estimation process, see Appendix A.

The noise levels were estimated to be as follows: i) 312.5 kHz - no field data for estimation, ii) 625 kHz -  $1.6 \cdot 10^{-6}$  V/m, iii) 1250 kHz:  $2.5 \cdot 10^{-6}$  V/m, iv) 2500 kHz:  $2.3 \cdot 10^{-5}$  V/m. It should be

noted that these noise level estimates were approximated using models with relative dielectric permittivity values that were greater than 1.

Using these values, Figure 23 was recalculated, and only the frequencies that had amplitude values that were above these noise levels were listed in the various regions (Figure 24). From this rough estimation, it can be seen that for this particular case, the signal may be too small when the conductivity of the material exceeds about  $10^{-3}$  S/m, due to noise overshadowing the signal.

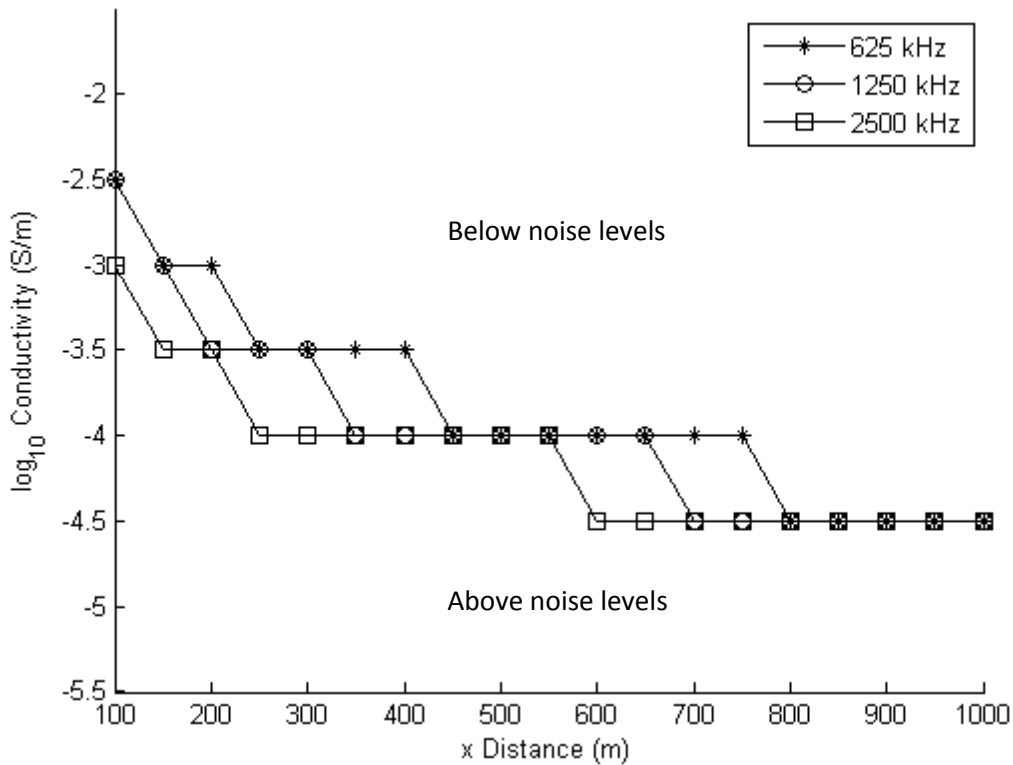


Figure 24. Conductivity versus  $x$  distance plot, showing the frequency in each region whose amplitude exceeds its roughly estimated noise level at that combination of values for the two parameters.

### 3.2.3 Angles

The effect of the angles of the boreholes was also investigated. As an example we looked at the cases when the receiver hole is tilted 20 degrees towards the transmitter hole, and when the transmitter hole is tilted 20 degrees towards the transmitter hole (Figure 25). The position of the peak and the amplitude of the peak changes as the angles of the boreholes increase (Figure 26).

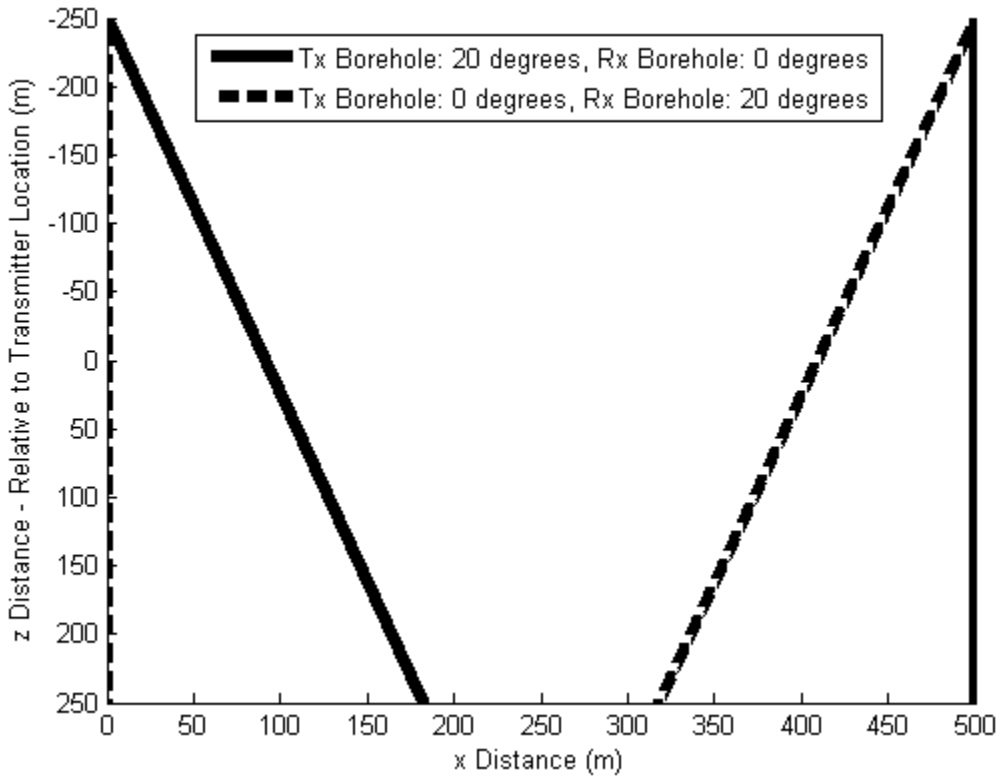


Figure 25. The two angled borehole geometries used for the simulations in Figure 26.

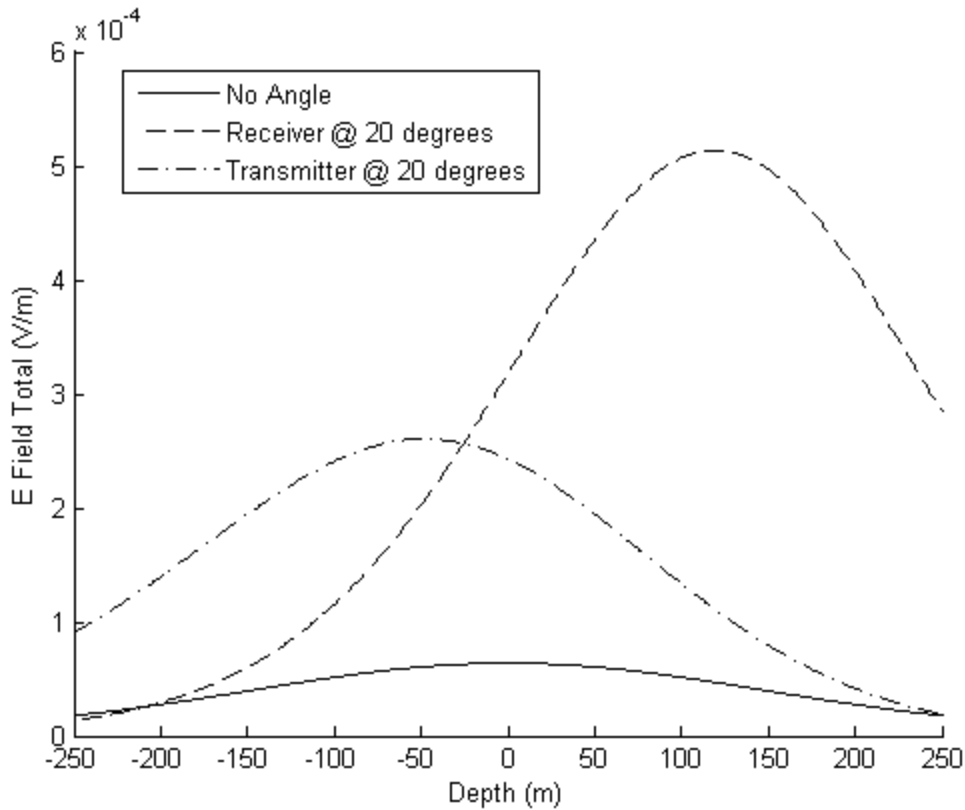


Figure 26. (top) A comparison of the amplitudes between a parallel borehole system (solid line), a system with the receiver borehole at an angle of 20 degrees (dash line), and a system with the transmitter borehole at an angle of 20 degrees (dash-dot line).

The amplitude peak value and position were calculated for a range of receiver and transmitter borehole angles (Figure 27). The amplitude of the peak increases as the angle increases, due to the boreholes moving closer to one another. Likewise, the position of the peak shifts up or down the borehole (for transmitter angle or receiver angle respectively), away from the point directly across from the transmitter. However this only occurs until approximately 30 degrees for the receiver borehole increase, and 20 degrees for the transmitter borehole increase, after which the

peak begins shifting back. This can be explained as an effect of the greater influence of the  $x$  component of the field, and will occur in different system geometries at different angles.

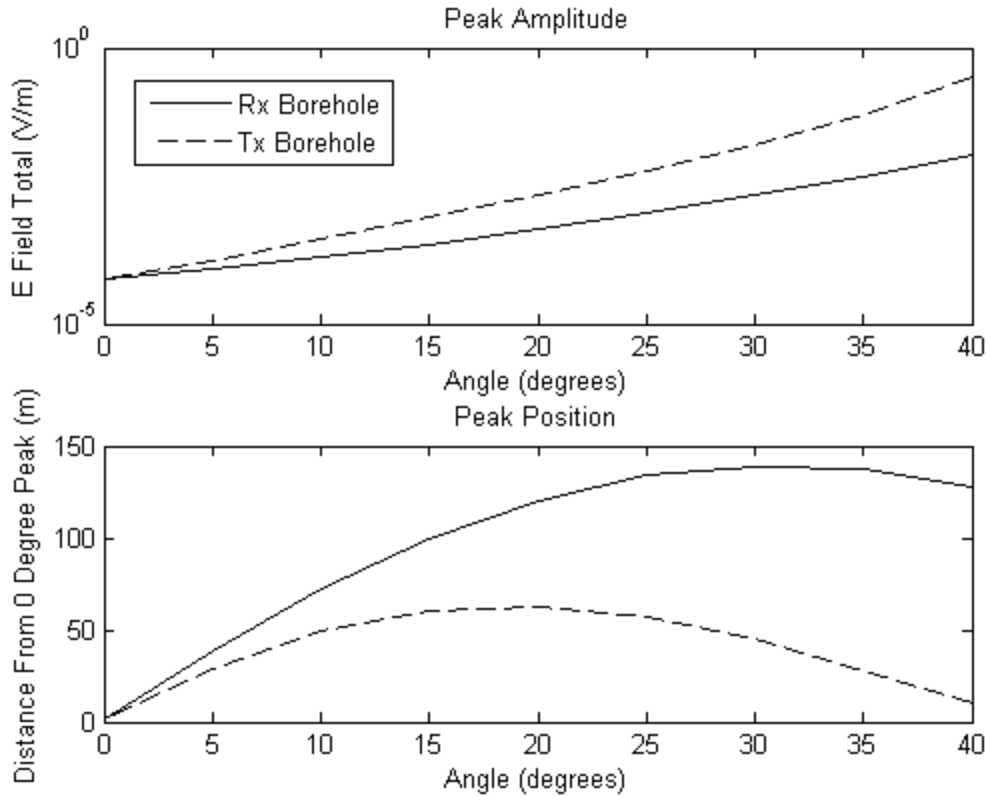


Figure 27. The peak amplitude and peak position as a function of the borehole angle. The peak position is measured with respect to the position directly across from the transmitter where the zero degree peak occurs. This is for a  $10^{-4}$  S/m whole space with the distance between boreholes set to 500m.

### 3.3 Discussion

The whole-space modelling program allows varying both the transmitter and receiver angles, which introduces even further complexity. With the ability to adjust the geometry, many systems can be modelled. Therefore, the greatest strength of this model is its ease of use in not only

investigating overarching patterns, but specific system configurations as well. The above investigation of the patterns that occur from the parameters is not all-encompassing, but instead has focused on several of the major parameters, and the general changes that occur with them. This study has shown how specific parameters may affect data, however more can be investigated and pursued if an understanding of a specific variation is required. For instance, with more work, one possible area of investigation would be creating empirical equations to some of these patterns. To do this, the modelling program could be used to generate a set of data that could be correlated to create an analytic equation relating the peak position (and other geometry) to the conductivity, such that, given a set of real data, an estimate for the conductivity of the material could be found using only the geometric factors and the resulting data.

There are many of these possibilities with this whole-space modelling program, and as such, this Parameter Investigation section should be seen primarily as an overview of the main parameters, and the effects they have on the resulting signal. For more specific inquiries, the program itself can be used.

#### **4 Survey from Drury, Sudbury**

To check the applicability of the whole-space model, we modelled field data from a survey in Drury Township, near Sudbury, Ontario, Canada. The data were collected by GEOFARA using the Fara RIM system on behalf of Sudbury Integrated Nickel Operations, a Glencore Company.

Figures 28, 29, and 30 show the conductivity tomograms created by GEOFARA. These plots show the conductivity between boreholes DR-151 and DR-160 for transmitter frequencies of 625

kHz, 1250 kHz, and 2500 kHz respectively. Two data sets were collected at these three frequencies: one set with the transmitter in DR-151 and the receiver in DR-160, and the reciprocal set with the transmitter and receiver switched.

As can be seen, the area is divided by material of higher resistivity above approximately -325 m, and material of lower resistivity below -325 m, with the greatest conductivity concentrated about -450 m, closer to DR-151. There is a second conductive zone at -600 m closer to DR-160, with a resistive zone separating these two zones. Comparing the three tomograms, it can be seen that there is an overall trend of decreasing resistivity (increasing conductivity) as the frequency increases. While it is most obvious in the very conductive zones (red and green), the resistive zone above -325 m (blue) also tends towards a lower resistivity in the 1250 kHz and 2500 kHz tomograms, as compared to the 625 kHz tomogram. Based on Figure 28, the area above -325 m would range in conductivity anywhere from  $2 \times 10^{-4}$  S/m to  $5 \times 10^{-4}$  S/m, with the shallower depths showing lower conductivity values. Below the -325 m depth there is a sharp increase in conductivity.

RIM tomography reconstruction  
Apparent resistivity, 625kHz

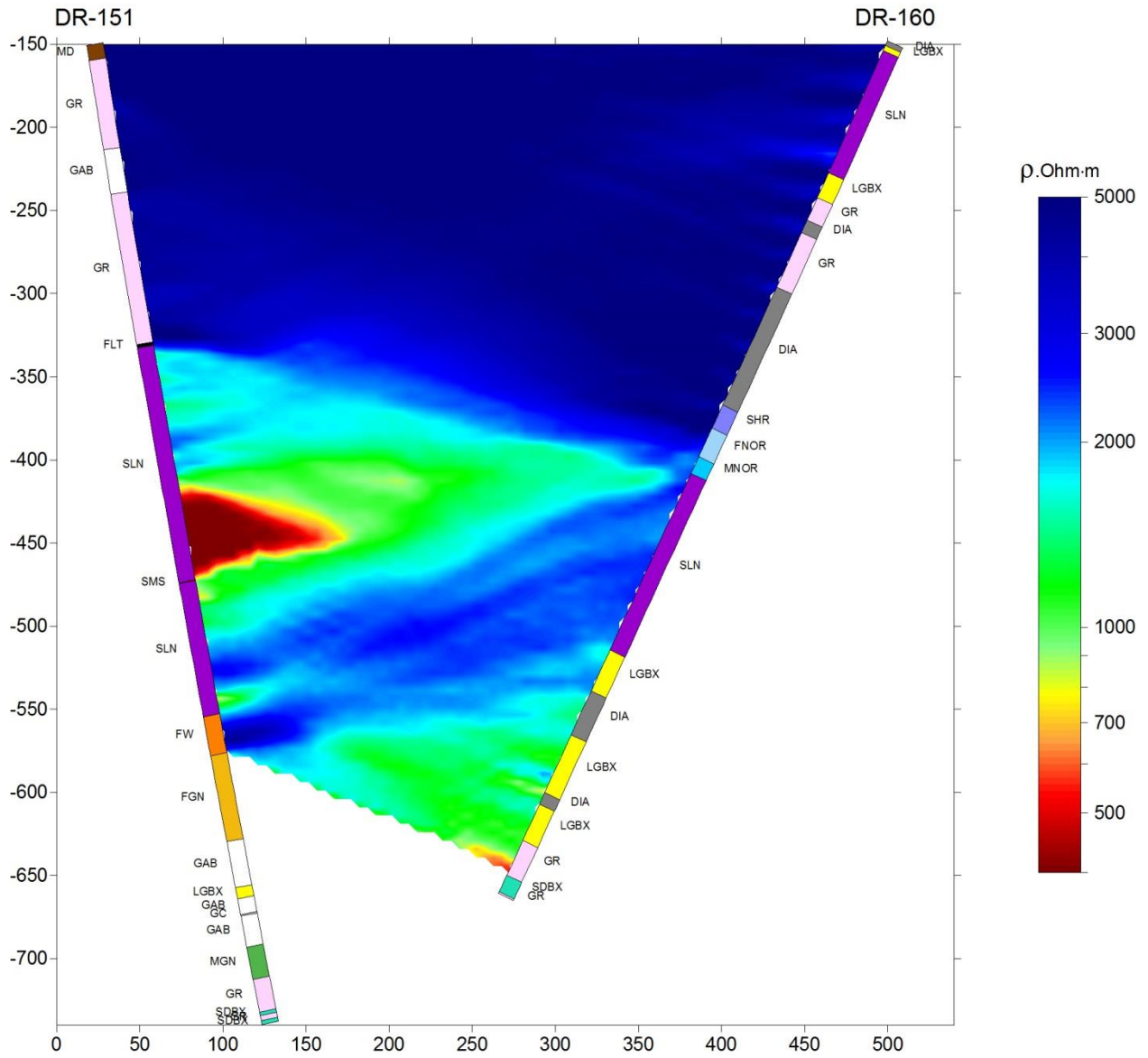


Figure 28. The 625 kHz resistivity tomogram.

RIM tomography reconstruction  
Apparent resistivity, 1250kHz

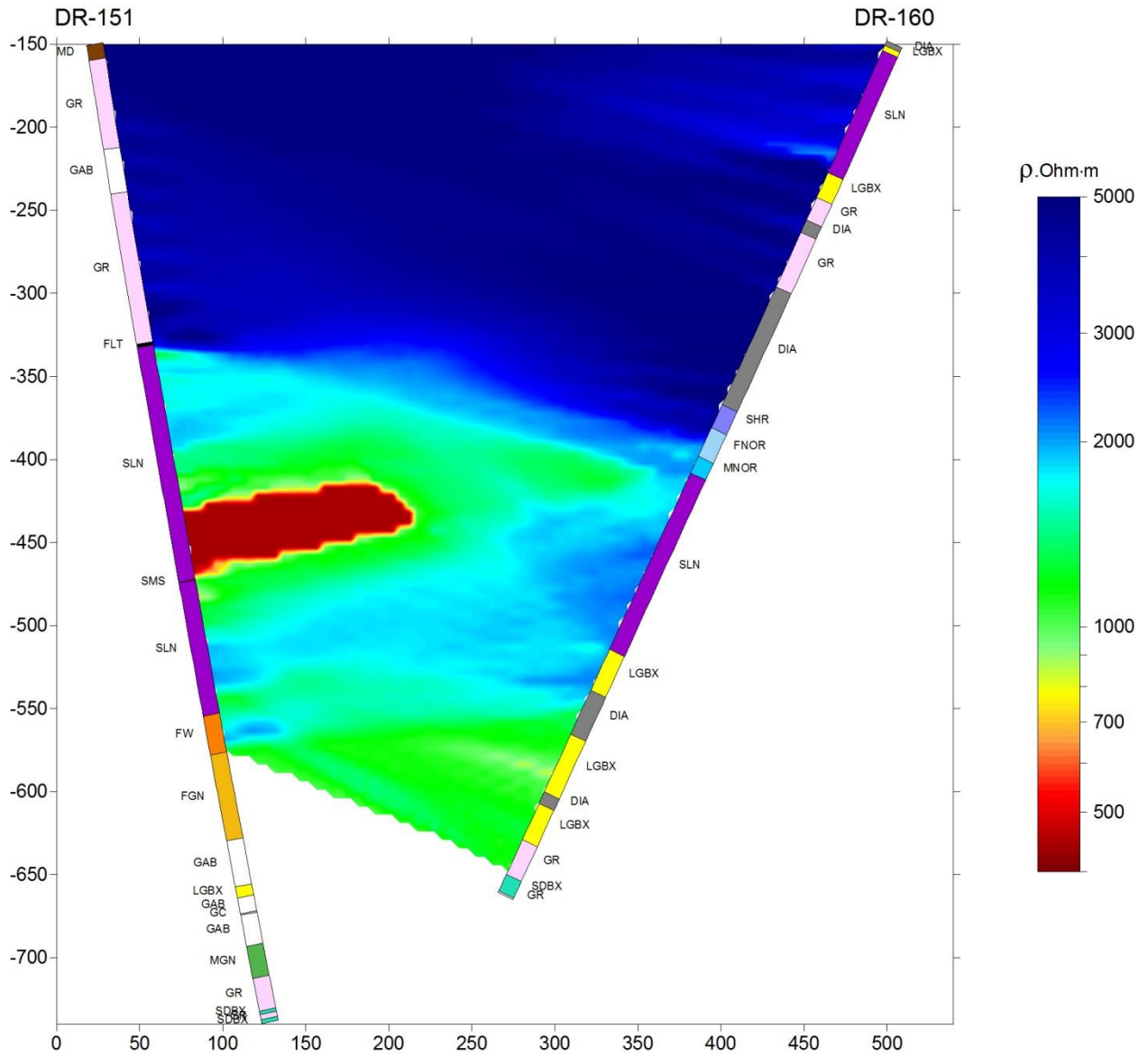


Figure 29. The 1250 kHz resistivity tomogram.

RIM tomography reconstruction  
Apparent resistivity, 2500kHz

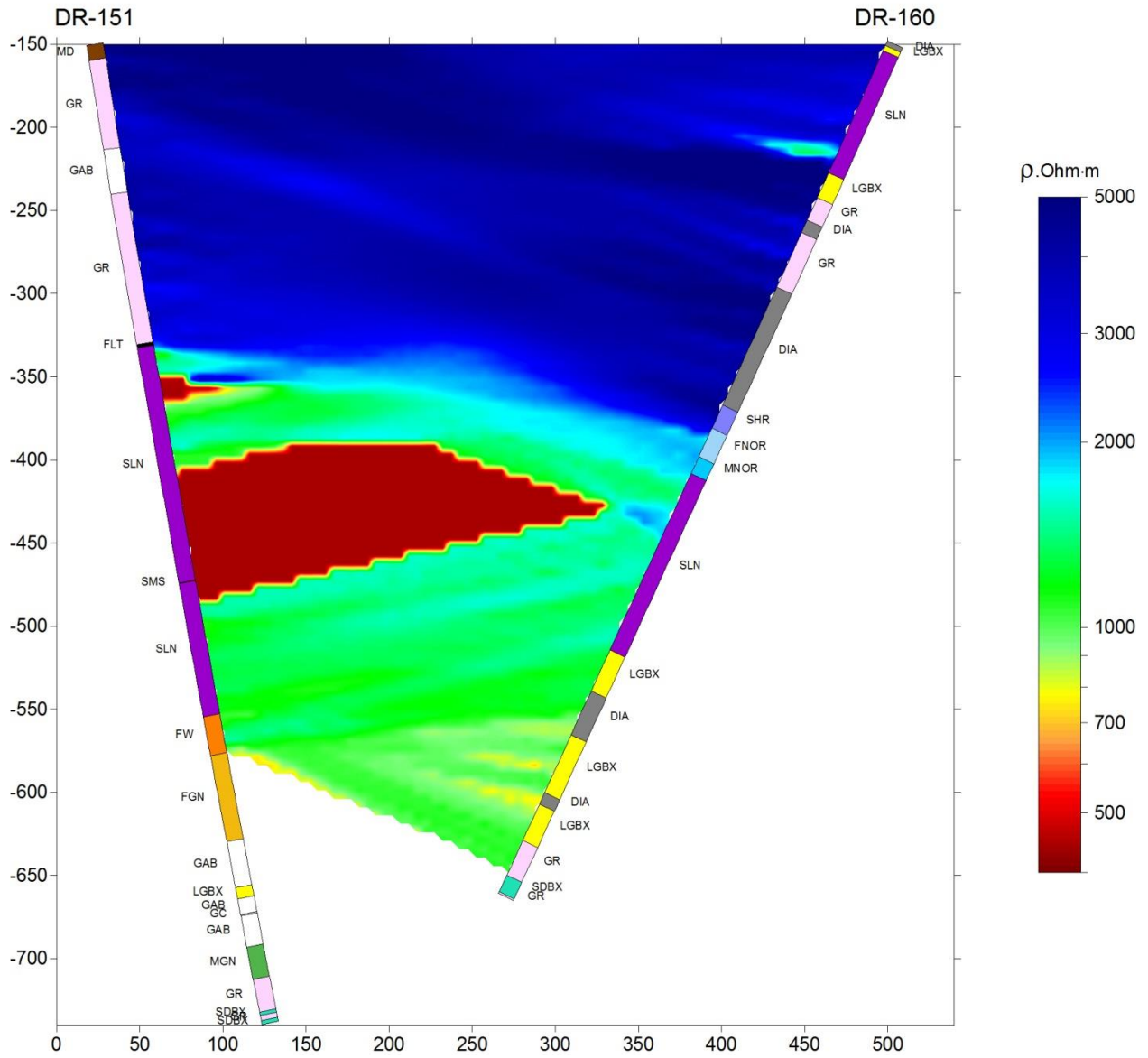


Figure 30. The 2500 kHz resistivity tomogram.

To recreate the data, the modelling program's parameters were made to represent the field situation as much as possible. The angles and distances were measured from the conductivity tomograms (Figures 28-30). The system geometry that was input into the program is shown in Figure 31.

The field data is organized by transmitter location. A location that was positioned in the resistive upper zone was chosen, as the signal is less attenuated, resulting in clearer data. Additionally, the upper resistive zone is fairly homogeneous, and therefore the modelling program should be able to recreate the data effectively using the whole-space model. Accordingly, the data set with the transmitter located at -275 m in borehole DR-160 was chosen for the case study.

Each transmitter location data set consists of amplitude and phase data for frequencies 625 kHz, 1250 kHz, and 2500 kHz. In recreating the data in the modelling program, each frequency data set was fit separately from the other frequencies. The conductivity was adjusted until the phase data peak position and sharpness matched that of the field data.

The phase data was used as the fitting method because the amplitude cannot be compared as easily as the phase data. The field data amplitude is measured in an uncalibrated amplitude unit, while the modelling program amplitude is measured in the physical units of the electric field (V/m). The overall amplitude and trends can still be compared. However, for fitting the conductivity, the phase data is much more effective.

The phase data collected by GEOFARA is exactly reversed in sign from the modelling program phase data. As such, for this case study, the modelling program phase has been multiplied by a factor of -1. Therefore all "rules of thumb" pertaining to phase described in the Parameter Investigation section must be inverted for explanations here.

When simulating the field measurements, the model data and the field data appeared to be shifted with respect to each other in the borehole depth. This was assumed to be due to slightly incorrect geometry from the assumptions that were used to recreate the situation in the model. These assumptions were that the boreholes were co-planar (in the same y-plane), and that the boreholes were drilled at a constant angle. All case study data has been shifted by -75 m (up the borehole) in depth.

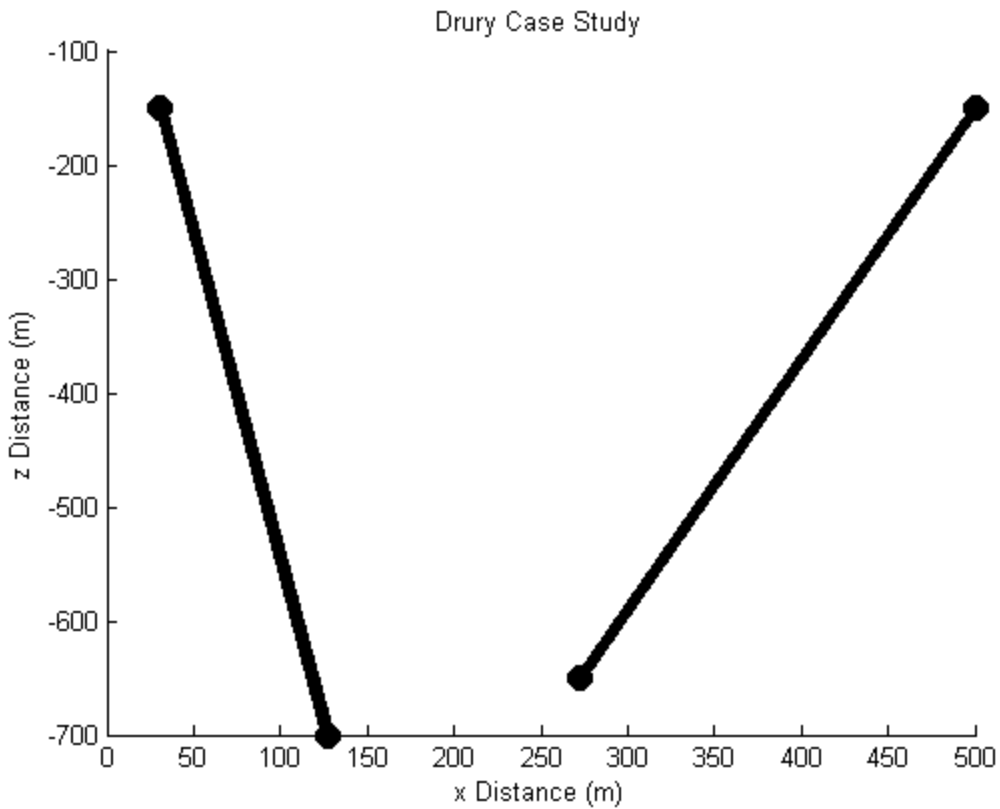


Figure 31. The modelling program recreation of the geometric system in the Drury RIM data collection.

Two sets of synthetic data were generated. In the first set, only the conductivity was varied. Figures 32, 33, and 34 show comparisons between the synthetic modelling program data and the field data, for transmitter frequencies of 625 kHz, 1250 kHz, and 2500 kHz respectively. The conductivities were set to  $2.1 \cdot 10^{-3}$  S/m,  $3 \cdot 10^{-3}$  S/m, and  $9 \cdot 10^{-3}$  S/m respectively for the three frequencies. The relative dielectric permittivity and relative magnetic permeability were both set to 1. Overall the three models fit well with the field data at shallow depths above 325 m; however the conductivities used are at least an order of magnitude greater than expected from the GEOFARA tomograms.

Note that the cusps seen in the synthetic data around the 400 m mark are due to the geometry of the system, such that the  $x$ -component of the electric field begins to dominate over the  $z$ -component of the electric field. This can be explicitly seen in Appendix B.

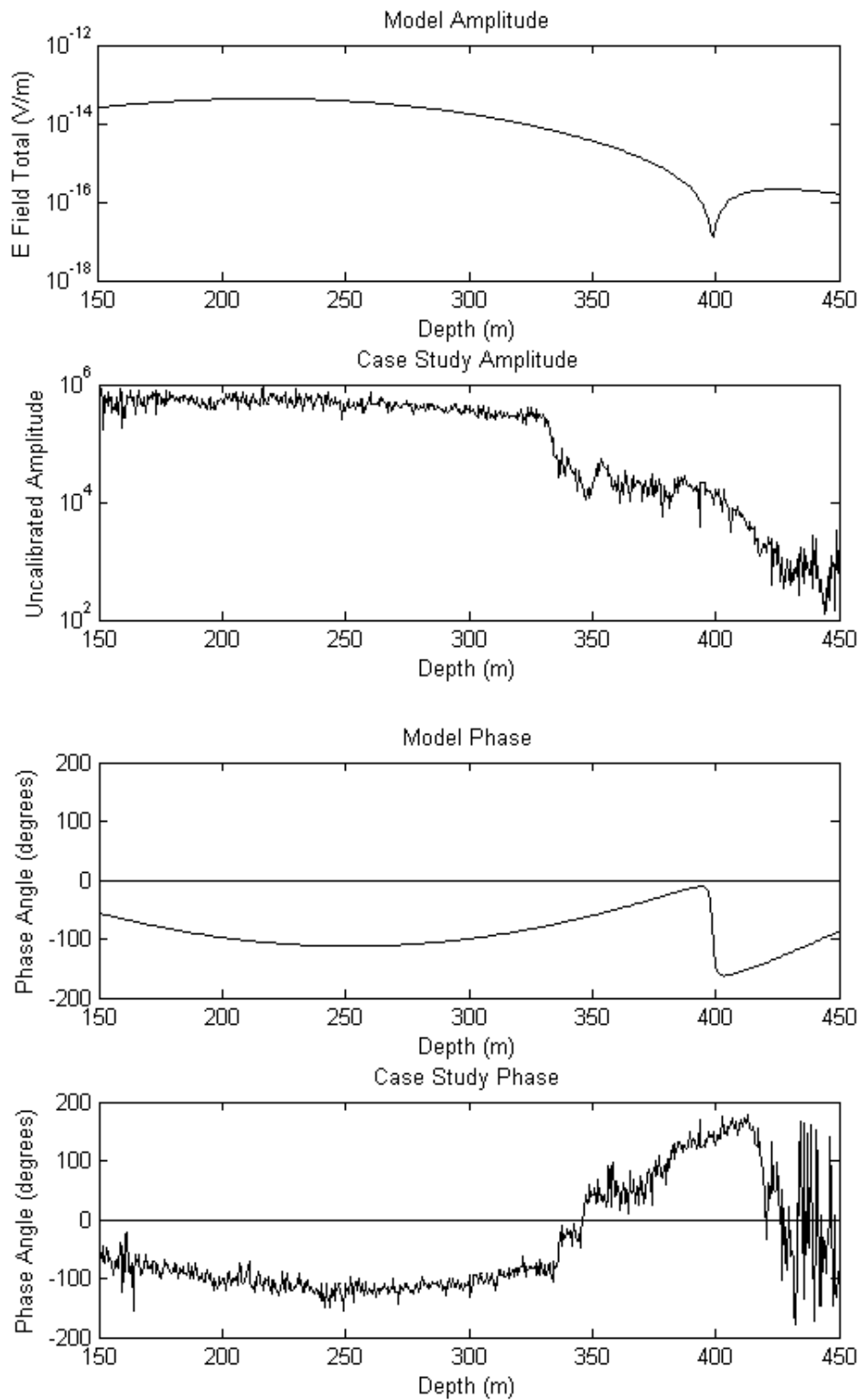


Figure 32. Model and real data comparisons, with the transmitter at -275 m in borehole DR-160, frequency = 625 kHz. The model conductivity is set to  $2.1 \cdot 10^{-3}$  S/m.

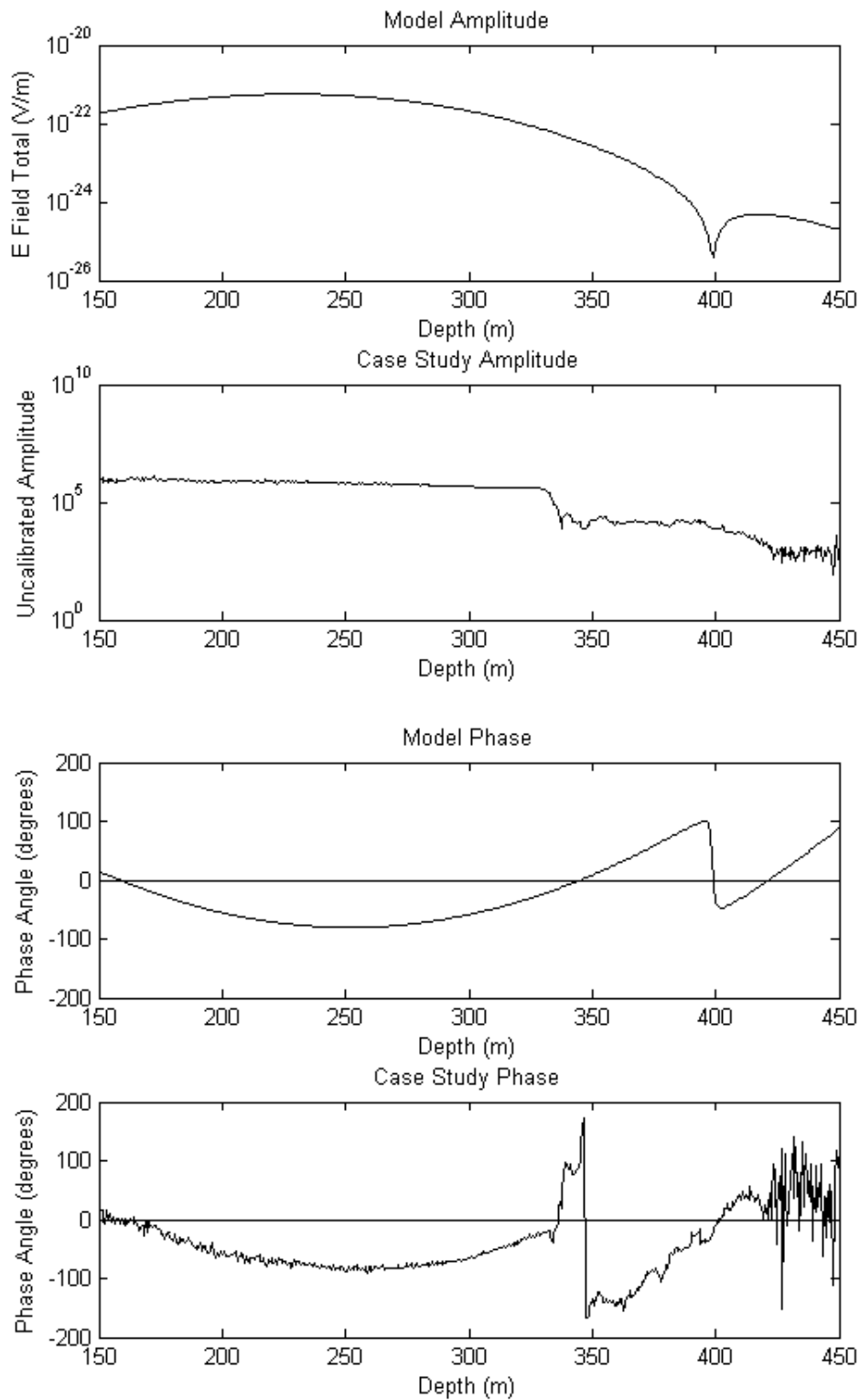


Figure 33. Model and real data comparisons, with the transmitter at -275 m in borehole DR-160, frequency = 1250 kHz. The model conductivity is set to  $3 \cdot 10^{-3}$  S/m.

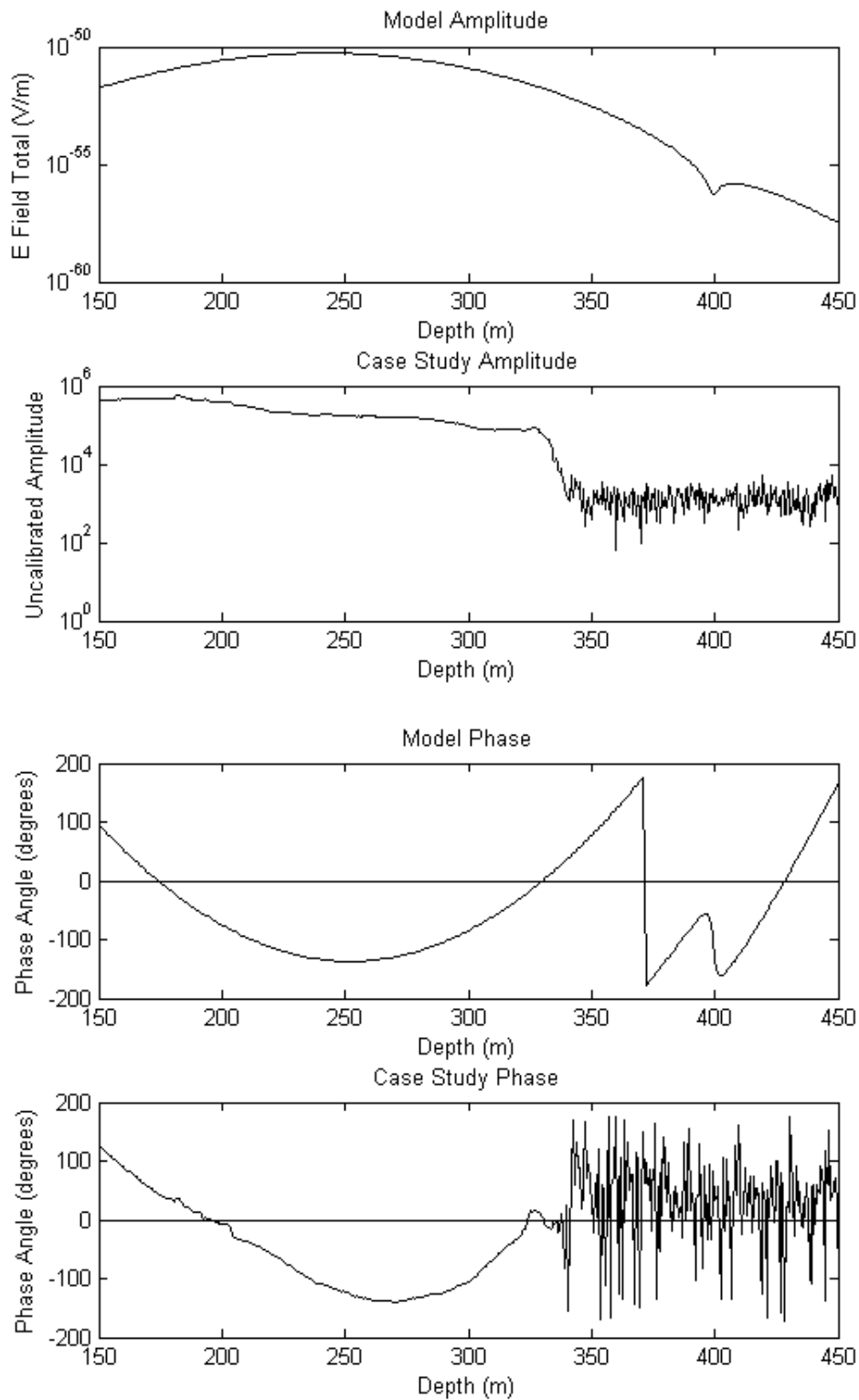


Figure 34. Model and real data comparisons, with the transmitter at -275 m in borehole DR-160, frequency = 2500 kHz. The model conductivity is set to  $9 \times 10^{-3}$  S/m.

In this set, two primary discrepancies can be seen.

The first discrepancy is simple to explain. Below the -325 m depth there is a sharp decrease in amplitude and a sharp increase in phase. Based on the information obtained in the Parameter Investigation section, this could be explained by a sudden increase in conductivity. This is consistent with the conductive zone evident on the GEOFARA tomograms.

The other discrepancy is somewhat more subtle. In Figures 32 and 33 (625 kHz and 1250 kHz) when the receiver in DR-151 is above the -250 m depth, as the depth decreases the field data amplitude falls off at a slower rate than the synthetic data, and its associated phase data increases towards 0 at a slower rate than the synthetic data. Both of these can be explained by a decrease in conductivity as also evident in the Parameter Investigation section. The tomograms in Figures 28 and 29 (625 kHz and 1250 kHz) show that there is a small increase in resistivity above -250 m near DR-151, and this is consistent with the observed behaviour in the measurements.

Above the -250 m depth, Figure 34 (2500 kHz) appears to show both a slight increase in measured amplitude, as well as a slight increase in the rate of change of measured phase. This is unlike the previous two cases, where the amplitude increased, but the phase rate of change was slowed. The GEOFARA tomogram (Figure 30) shows an increase in resistivity, similar to the other tomograms. So while the 2500 kHz synthetic data (Figure 34) still fits fairly well, there is another possible explanation: the amplitude and phase variation might be indicative of a possible increase in dielectric permittivity. As seen in the Parameter Investigation section, an increase in amplitude, a reduction in the phase amplitude (or for the field data, an increase), and a sharpening of the phase peak can be explained by an increase in dielectric permittivity. As explained in Appendix C, the dielectric permittivity affects higher frequencies more drastically than lower frequencies, and therefore by increasing the relative dielectric permittivity, this

discrepancy may be explained. Additionally, increasing the dielectric permittivity will increase the amplitude values in all three frequency cases.

As such, another set of synthetic data were generated, setting the conductivity in the range expected from the tomograms (approximately  $3 \cdot 10^{-4}$  S/m), followed by increasing the dielectric permittivity. Figures 35 to 37 show these new data plots. The relative dielectric permittivity values were set to 19.5, 17.3, and 18 for 625 kHz, 1250 kHz, and 2500 kHz respectively. It can be seen that the synthetic amplitude plots are closer to the measured data, primarily above the 225 m point, as compared to the previous set of data. The phase data still fits well and has not changed significantly from the previous data.

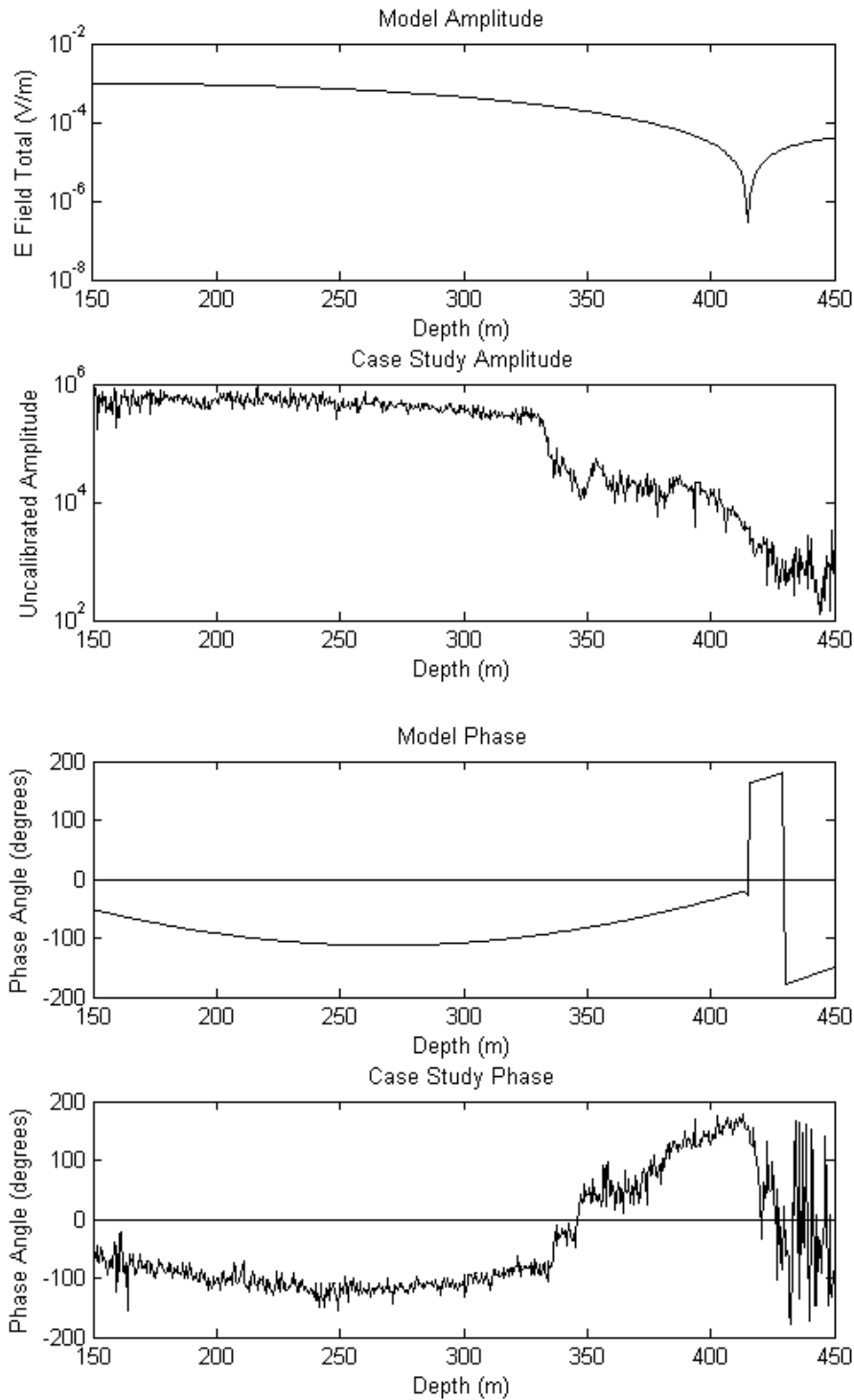


Figure 35. Model and real data comparisons, with the transmitter at -275 m in borehole DR-160, frequency = 625 kHz. The model conductivity is set to  $3 \cdot 10^{-4}$  S/m, and the relative dielectric permittivity is set to 19.5.

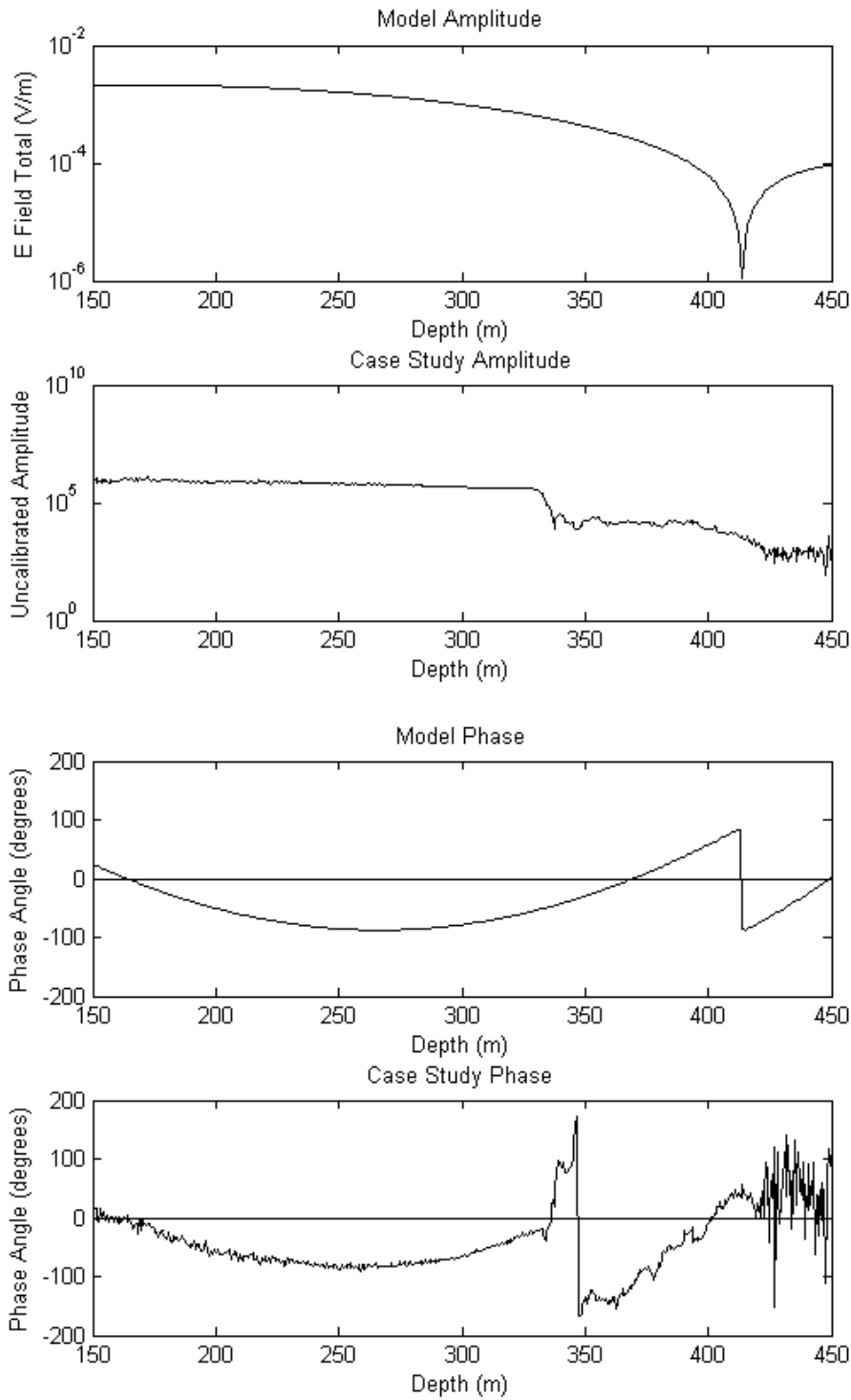


Figure 36. Model and real data comparisons, with the transmitter at -275 m in borehole DR-160, frequency = 1250 kHz. The model conductivity is set to  $3 \cdot 10^{-4}$  S/m, and the relative dielectric permittivity is set to 17.3.

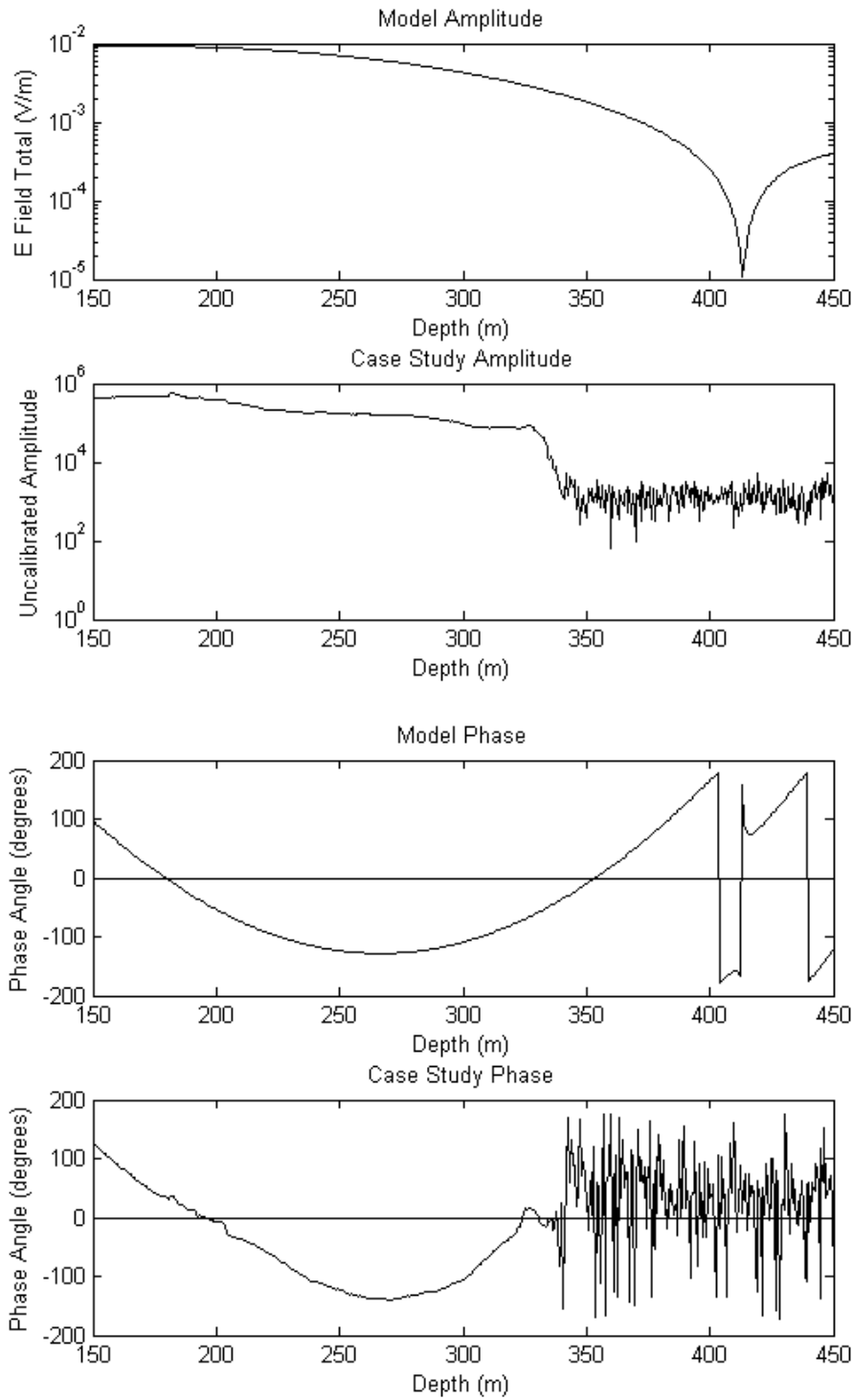


Figure 37. Model and real data comparisons, with the transmitter at -275 m in borehole DR-160, frequency = 2500 kHz. The model conductivity is set to  $3 \cdot 10^{-4}$  S/m, and the relative dielectric permittivity is set to 18.

From this case study, it can be concluded that the whole-space model may be used to simulate real data effectively. Despite it being a homogeneous model, it can recreate sections of field data, and the discrepancies between the model and the field data can be explained by inhomogeneity in the physical properties, where the profiles diverge from those that are expected.

The difference between the case of synthetic data where only the conductivity was varied, and the other case where conductivity was set to the expected value and dielectric permittivity was varied, illustrates that the RIM method is sensitive to permittivity and that RIM modelling programs should take permittivity into account.

## **5 Forward Modelling Program**

A GUI was built in Matlab for the modelling program, primarily for ease of use while conducting both the Parameter Investigation as well as the Case Study. After realizing its potential uses in quality assurance/quality control (QA/QC) as a forward model, the program was ported to the Python language, such that it could be run without the need of the Matlab software. As such, this program (Figure 38) is to be considered as a deliverable from this M.Sc. thesis.

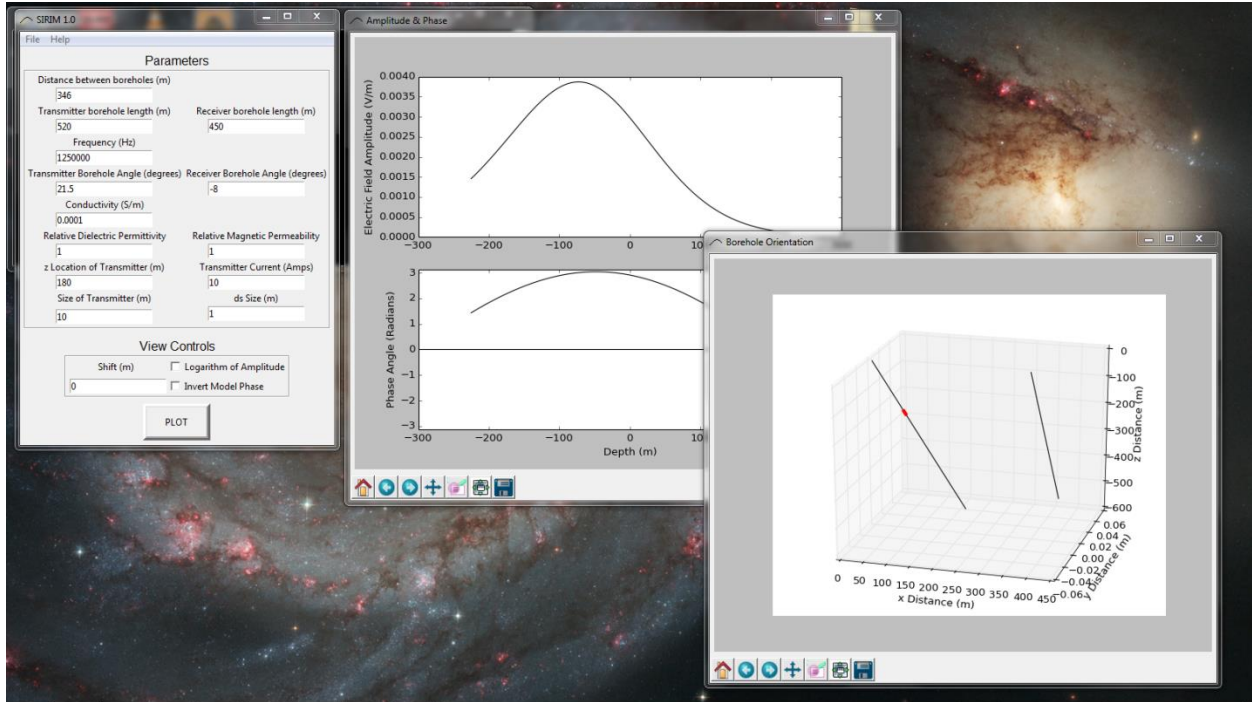


Figure 38. An example of the Python GUI.

It allows variation of the system parameters, and will plot the amplitude, phase, and system geometry. A system can be saved and loaded for later use, as well as exported as values such that a model can be plotted and manipulated in another program if desired. To operate it as a forward model, a dataset may be loaded into the program, and then the system parameters manipulated until the desired fit of the synthetic data is found (Figure 39).

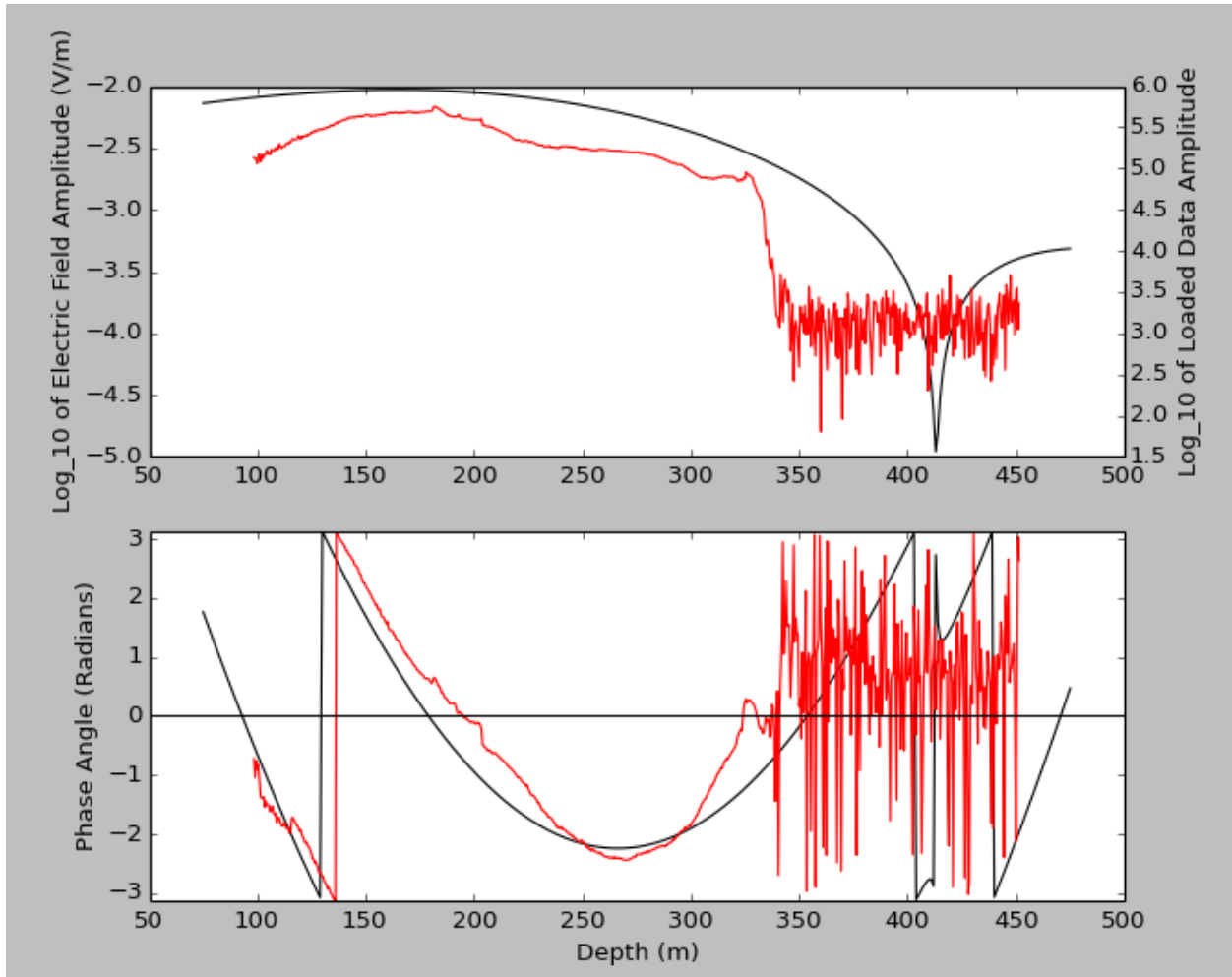


Figure 39. An example of the forward model capability of SIRIM. The black line is the synthetic data, and the red line is the imported field data.

## 6 Conclusions

The formula for the electric field of a dipole in a whole space can be used to simulate the response as measured by the radio imaging method. By varying a set of input parameters, a better understanding of how the RIM amplitude and phase signal change has been obtained.

The use of the transmitter as an infinitesimal dipole is appropriate for calculations in almost all situations. However in particularly conductive environments or configurations with small borehole offsets, modelling the transmitter as two half-sized dipoles will remove most of the error that could arise from incorrectly specifying the transmitter geometry.

A parameter investigation varied the input parameters (borehole offset, conductivity, dielectric permittivity, and magnetic permeability) and key changes in the response were observed, resulting in a set of “rules of thumb” as to how the amplitude and phase of the RIM signal is expected to vary. These rules state that, in general, when increasing any of these four parameters, predictable patterns in the value and shape of the amplitude and phase data can be expected. Increasing the borehole separation causes both amplitude and phase peaks to broaden, decreases the amplitude value, and shifts and the phase value negatively. Increasing the conductivity causes similar changes, except the amplitude and phase peaks sharpen. Increasing the dielectric permittivity causes the amplitude peak to broaden slightly, the phase peak to sharpen, and increases amplitude values, but shifts phase values negatively. Increasing the magnetic permeability causes the amplitude and phase peaks to sharpen, decreases the amplitude value, and shifts the phase value negatively.

The effectiveness of different frequencies in various systems was investigated. As would be expected, it was found that at smaller distances and in more resistive material, higher frequencies would result in the highest amplitude, while at larger distances and more conductive systems, lower frequencies result in significantly greater amplitudes. The magnitude to which these generalities occurred was quantified: at distances greater than 300 metres and conductivities

greater than  $10^{-4}$  S/m, lower frequencies dominated in effectiveness, as higher frequencies have small amplitudes at these greater distances and conductivities.

Finally, an investigation of the effect of borehole angles showed that angles have a complex effect on the signal, both “shifting” the data as well as increasing or decreasing the amplitude value. These geometric effects should be taken into account in modelling so that their effects are not misattributed to other factors such as the physical properties of the material.

The modelling program created was shown to be an effective forward model for RIM data. Using data taken in Drury Township, near Sudbury, Ontario, Canada, field data from the more resistive part of the hole was simulated in the modelling program with success. When forward modelling field data, the whole-space model is effective at simulating measured data where both the transmitter and receiver are in material that is uniformly conductive. The differences between the model data and the field data can be explained and understood as variability in the conductivity, and possibly the dielectric permittivity. The model was adjusted with the knowledge gained from the parameter investigation. It was found that fitting with the phase data, and not the amplitude, was much more effective when finding the appropriate conductivity value.

The whole-space modelling program can be effective as an investigative tool to better understand how the RIM signal changes due to varying parameters, and for the forward modelling of real data. As such a user-friendly version of the program was developed in Python for easy use and distribution.

The ambiguity between conductivity and magnetic permeability may require further investigation to gain a solid understanding of differing responses to changes in these two system parameters. Additionally, further analysis of the effect of angles on the response may prove to be beneficial. As such, it is recommended that these two issues be further studied.

It is finally recommended that the modelling program be further developed to include a y-axis offset, as this may help account for errors due to geometry, such as the -75 m shift required in the case study.

## 7 References

Fullagar, P., D. Livelybrooks, P. Zhang, A. Clavert, and Y. Wu, 2000, Radio tomography and borehole radar delineation of the McConnell nickel sulfide deposit, Sudbury, Ontario, Canada *Geophysics*, 65, 1920–1930.

Holliger, K., Musil, M., Maurer, H.R., 2001, Ray-based amplitude tomography for crosshole georadar data: a numerical assessment, *Journal of Applied Geophysics*, 47, 285–298.

Jang, H., M. Park, and H. Kim, 2006, Numerical modeling of antenna transmission for borehole ground-penetrating radar, *Proceedings of the 8th SEGJ International Symposium*, 1-6.

Johnson, D., 1997, Finite Difference Time Domain Modelling of Cross-Hole Electromagnetic Survey Data: M.S. thesis, University of Utah.

Karimi Sharif, L., 2013, Application of the cross-hole Radio Imaging Method in detecting geological anomalies, MacLennan Township, Sudbury Ontario: M.S. thesis, Laurentian University.

Korpisalo A., Heikkinen E., 2014, Radiowave imaging research (RIM) for determining the electrical conductivity of the rock in borehole section OL-KR4-OL-KR10 at Olkiluoto, Finland, *Exploration Geophysics*, <http://dx.doi.org/10.1071/EG13057>.

Livelybrooks, D., Chouteau, M., Zhang, P., Stevens, K., and Fullagar, P., 1996, Borehole radar and radio imaging surveys to delineate the McConnell ore body near Sudbury, Ontario, SEG Technical Program Expanded Abstracts, 2060-2063.

Mutton, A.J., 2000. The application of geophysics during evaluation of the Century zinc deposit, *Geophysics*, vol. 65, no. 6, 1946-60.

Pears G.A., P.K. Fullagar, 1998, Weighted tomographic imaging of radio frequency data, *Exploration Geophysics*, 29, 554–559.

Stevens, K., Watts, A. and Redko, G., 2000. In-Mine Applications of the Radio-Wave Method in the Sudbury Igneous Complex. Paper presented at the 2000 SEG Annual Meeting.

Stolarczack, L. G., Fry, R. C., 1986, Radio imaging method (RIM) or diagnostic imaging of anomalous geologic structures in coal seam waveguides. *Transactions of the Society for Mining, Metallurgy, and Exploration, Inc.*, 288, 1806-1814.

Thomson, S., J. Young, and N. Sheard, 1992, Base metal applications of the radio imaging method. Current status and case studies, *Exploration Geophysics*, 23, 367–372.

Ward, S. H., and G. W. Hohmann, 1987, Electromagnetic theory for geophysical applications, in M. N. Nabighian, ed., *Electromagnetic methods in applied geophysics I*: SEG, 131-312.

Zhou B., Fullagar P. K., Delineation of sulphide ore-zones by borehole radar tomography at Hellyer Mine, Australia, *Journal of Applied Geophysics*, 47, July 2001, 261-269.

Zhou, B., Fullagar, P.K. and Fallon, G.N., 1998. Radio frequency tomography trial at Mt Isa Mine. *Exploration Geophysics*, vol. 29, no. 3-4, 675-679.

## **Appendix A: Noise Level**

To get the noise level approximations used in section 3.2.2 Frequency Variation, the following process and calculations were completed.

Noise may vary from survey to survey, however an approximation can be found by comparing real data with synthetic data. To do this, data from the Drury County survey (used in the Case Study section) was analyzed to find noise levels for each of the three frequencies used in the survey.

The Fara RIM amplitude is measured in a form of uncalibrated amplitude values and not in the electric field units V/m. To convert the uncalibrated values to V/m, the field measurements were simulated in the modelling program as in the Case Study section, and several values were compared between the two data sets (Figure 40). It is important to note that the simulations used varied values of the dielectric permittivity, and could affect the precision of the results in this analysis.

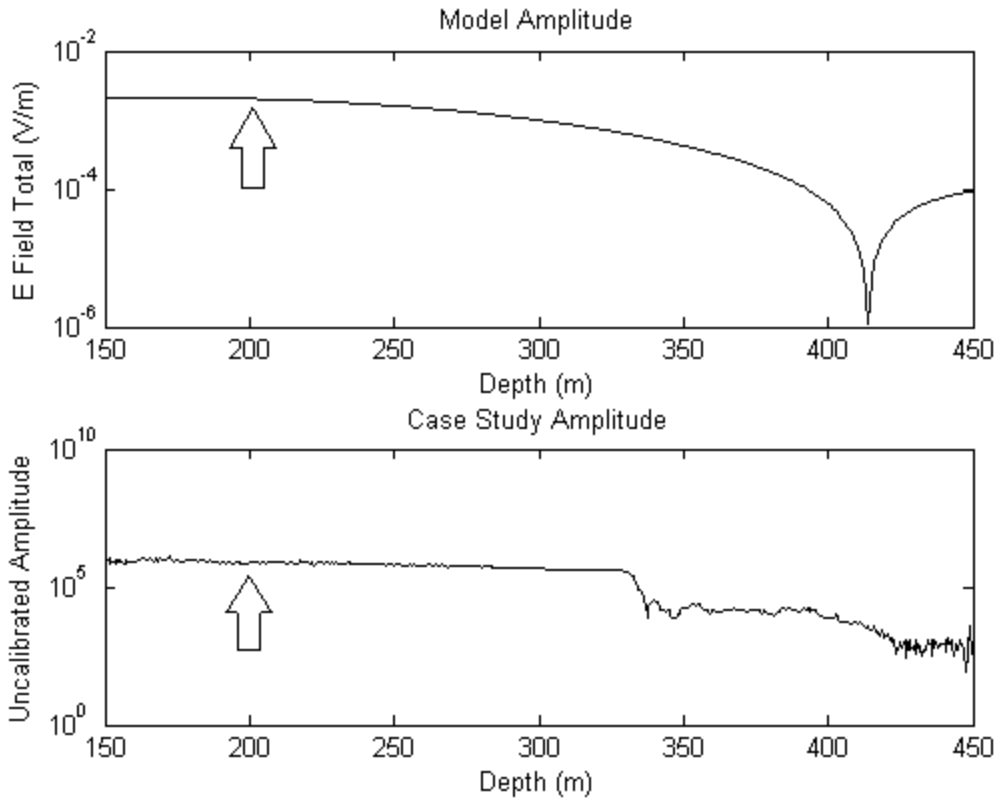


Figure 40. Example of the comparison of the synthetic data amplitude and the field data amplitude with the transmitter at -275 m in borehole DR-160, frequency = 1250 kHz. The model conductivity is set to  $3 \cdot 10^{-4}$  S/m, and the relative dielectric permittivity is set to 17.3. The arrows show the points of comparison used.

To convert the field data to units of V/m, a direct linear comparison is used:

$$\text{Field Data} = A * \text{Synthetic Data} \tag{14}$$

Where A is a constant to be determined.

By calculating the constant A, and knowing the uncalibrated field value where the noise overcomes true signal, a noise level in V/m can be found. Due to the many factors involved in this process (such as noise level variance and transmitter current amperage in the modelling program), these noise levels calculated should be seen as rough approximations used only to assist in the frequency analysis section of this thesis.

To find the approximate noise level in uncalibrated data, the point at which the noise overcomes the true signal was measured on several sets of field data, in all three frequencies (example in Figure 41). It was found that the field data fell into noise at approximately  $10^3$  uncalibrated units at all frequencies.

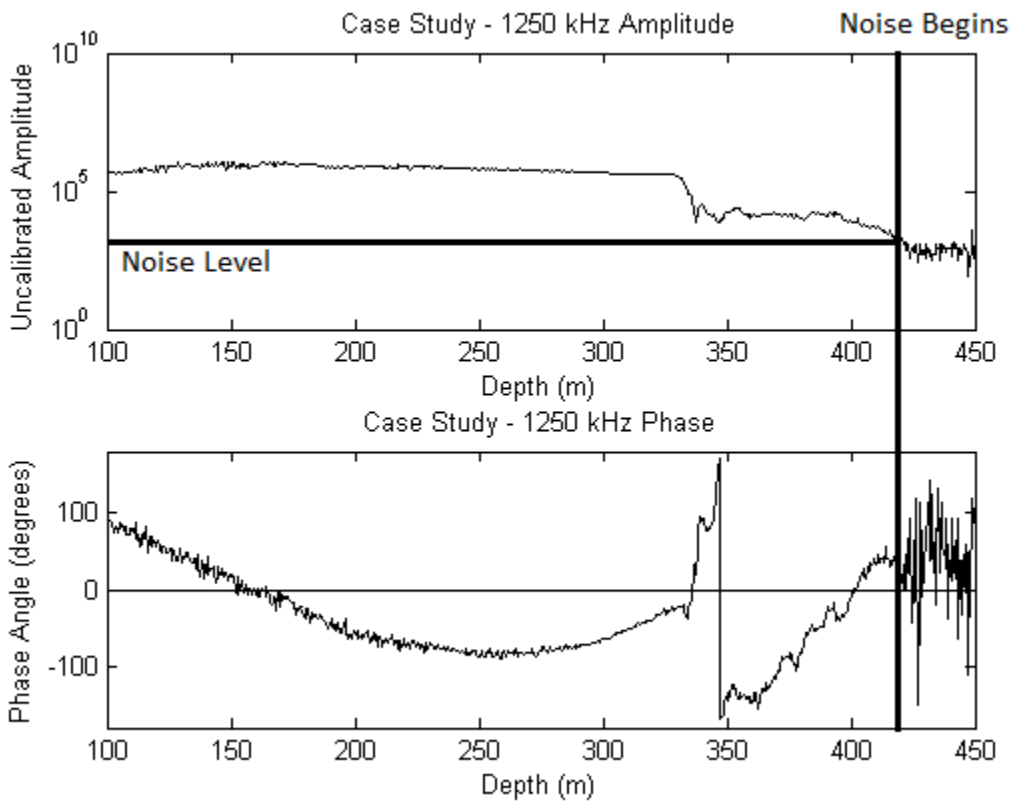


Figure 41. Example of the noise level estimate, using the 1250 kHz data with the transmitter at - 275 m in borehole DR-160. Noise here is at approximately  $10^3$  uncalibrated units.

Below are noise level calculations for each of the three frequencies used in the field data set (625 kHz, 1250 kHz, and 2500 kHz). 312.5 kHz was not used in the field data set, and as such, is not used here.

*625 kHz*

Synthetic Data – 0.0008911 V/m

Field Data –  $5.465 \times 10^5$  field units

Therefore  $A = 6.133 \times 10^8$  field units/V/m

Using the noise level as  $10^3$  field units equals approximately  $1.6 \times 10^{-6}$  V/m.

*1250 kHz*

Synthetic Data – 0.002031 V/m

Field Data –  $8.004 \times 10^5$  field units

Therefore  $A = 3.941 \times 10^8$  field units/V/m

Using the noise level as  $10^3$  field units equals approximately  $2.5 \times 10^{-6}$  V/m.

*2500 kHz*

Synthetic Data – 0.008878 V/m

Field Data –  $3.912 \times 10^5$  field units

Therefore  $A = 4.406 \times 10^7$  field units /V/m

Using the noise level as  $10^3$  field units equals approximately  $2.3 \times 10^{-5}$  V/m.

## Appendix B: Case Study Synthetic Data Cusps

Cusps appear near the 400 m depth in the synthetic data of the case study. The reason for these cusps is not immediately obvious, however breaking the total amplitude down into its components can reveal why this occurs. Figures 42 and 43 show the components of the synthetic data from Figure 32 (625 kHz, 2.1 S/m). Figure 42 shows the amplitude broken down into the (unsquared) real and imaginary components. Near the 400 m mark both components dip in magnitude. This can be better understood by viewing the amplitude in the measured  $z$  and  $x$  components (Figure 43). Near the 400 m mark, the  $x$  component of the electric field that is measured by the receiver begins to dominate, and the cusp point is where the crossover occurs.

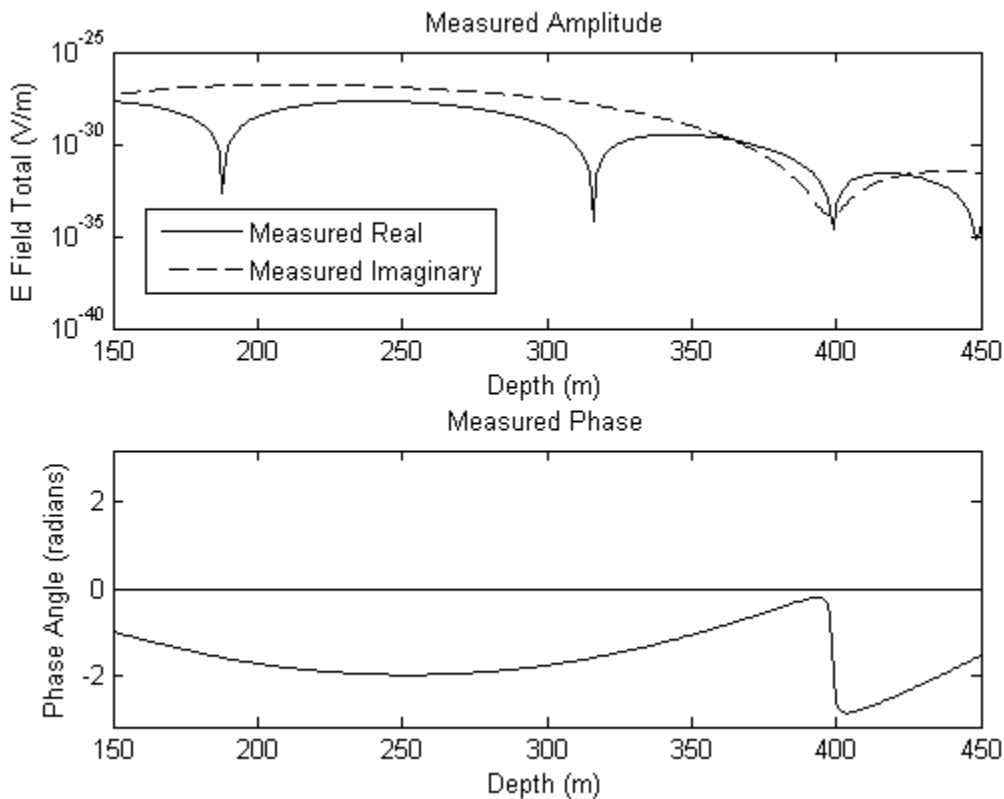


Figure 42. The measured real and imaginary components for the synthetic data from Figure 32.

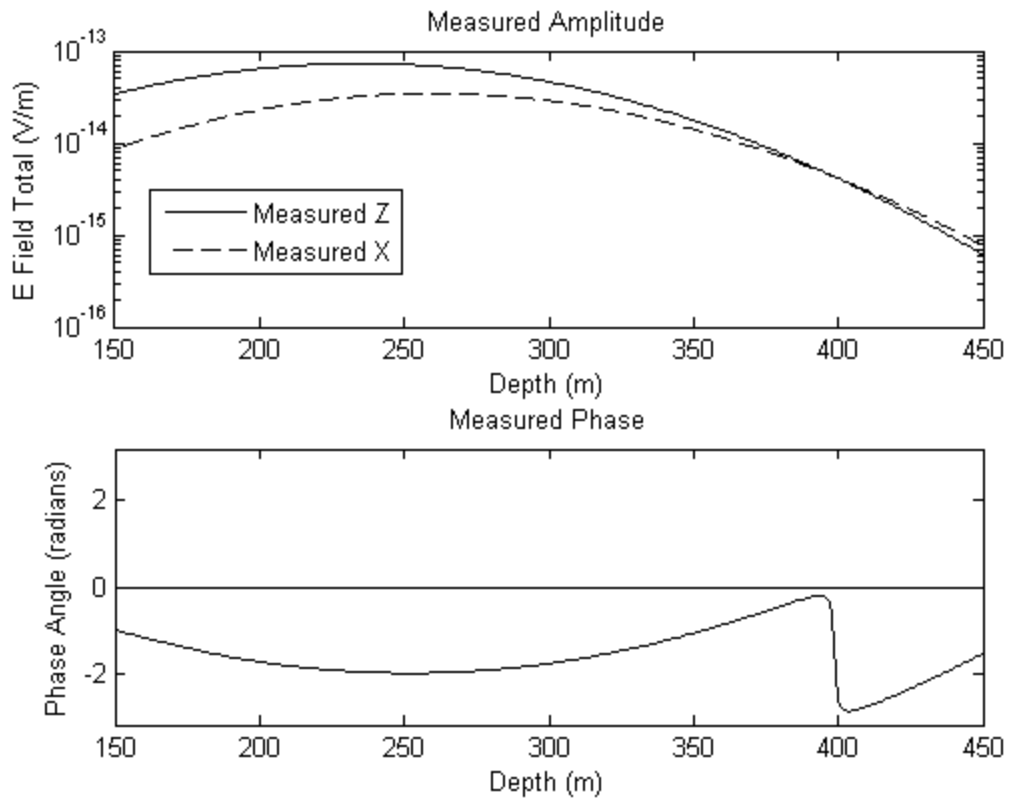


Figure 43. The measured  $z$  and  $x$  components for the synthetic data from Figure 32.

## **Appendix C: Frequency and Dielectric Permittivity**

Similar to the distance and conductivity range plots (Figures 20 and 21), a plot of the peak amplitudes over a range of dielectric permittivity values was built with the whole-space modelling program (Figure 44). From this, it can be seen that increasing values of the dielectric permittivity increases the amplitude in all cases; however the affects at higher frequencies are more drastic than the lower frequencies. This is also the case for the corresponding phase part of the signal.

Increasing or decreasing the conductivity and re-calculating this data shows the same trend of higher frequencies being affected more, combined with the effect of the conductivity change (Figures 45 and 46). As expected, a lower conductivity results in the amplitude of the higher frequencies being greater than the amplitude of the lower frequencies (Figure 45). A greater conductivity results in the amplitude of the lower frequencies being greater than the amplitude of the higher frequencies; however, as the relative dielectric permittivity increases, the higher frequencies' amplitudes increase at a much greater rate than the amplitudes of the lower frequencies (Figure 46).

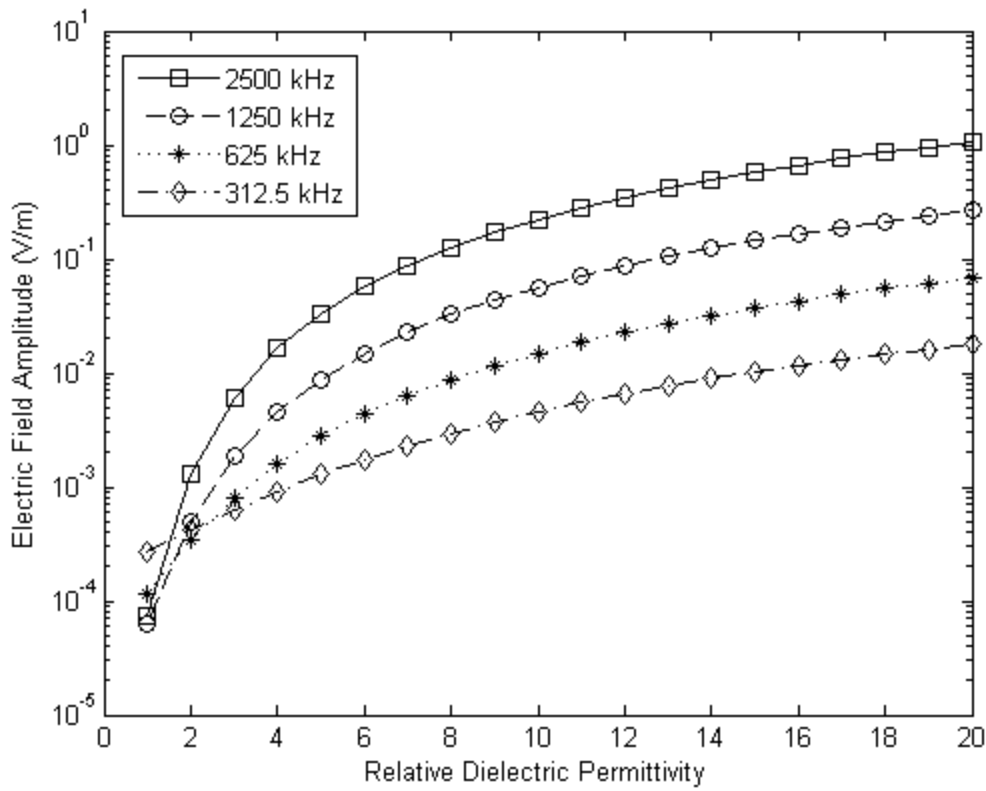


Figure 44. The peak amplitudes of four frequencies as a function of the relative dielectric permittivity. This is for a parallel borehole system, with the distance between boreholes set to 500 m, and a conductivity of  $10^{-4}$  S/m.

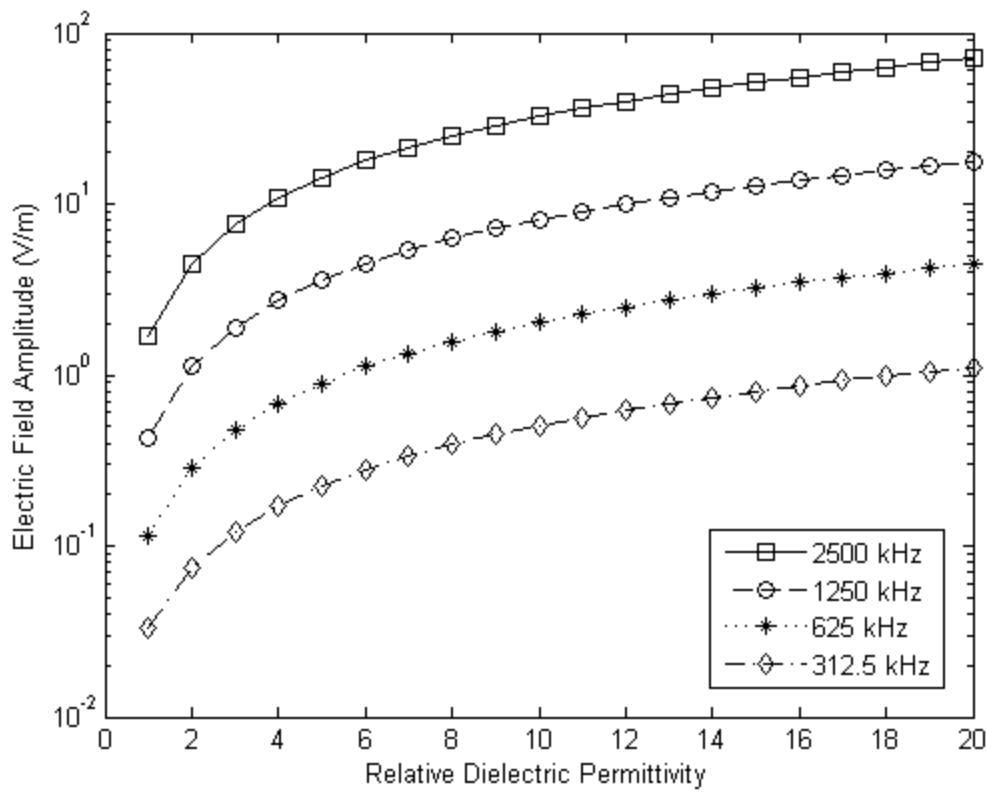


Figure 45. The peak amplitudes of four frequencies as a function of the relative dielectric permittivity. This is for a parallel borehole system, with the distance between boreholes set to 500 m, and a conductivity of  $10^{-5}$  S/m.

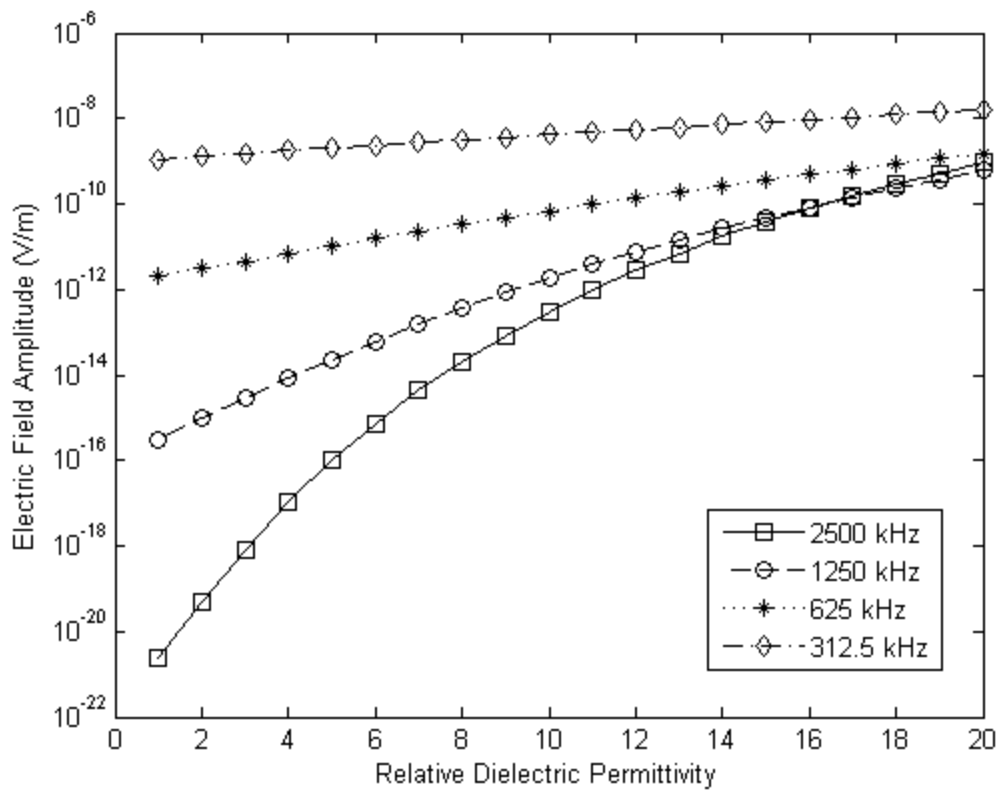


Figure 46. The peak amplitudes of four frequencies as a function of the relative dielectric permittivity. This is for a parallel borehole system, with the distance between boreholes set to 500 m, and a conductivity of  $10^{-3}$  S/m.